Received: 11 August 2022 | Revised: 10 October 2022 | Accepted: 17 October 2022

DOI: 10.1002/appl.202200070

MINI REVIEW

Applied Research

V_2O_5 as a versatile electrode material for postlithium energy storage systems

Qiang Fu[1] | Hainan Zhao[1,2] | Angelina Sarapulova[1] | Sonia Dsoke[1]

[1]Institute for Applied Materials (IAM), Karlsruhe Institute of Technology (KIT), Eggenstein-Leopoldshafen, Germany

[2]Key Laboratory of Physics and Technology for Advanced Batteries (Ministry of Education), College of Physics, Jilin University, Changchun, People's Republic of China

Correspondence
Qiang Fu, Institute for Applied Materials (IAM), Karlsruhe Institute of Technology (KIT), Hermann-von-Helmholtz-Platz 1, D-76344 Eggenstein-Leopoldshafen, Germany.
Email: qiang.fu@kit.edu

Funding information
China Scholarship Council, Grant/Award Number: 202006170127; Deutsche Forschungsgemeinschaft, Grant/Award Number: ProjectID390874152

Abstract

Postlithium batteries have received intense attention as an alternative for large-scale electric energy storage systems due to their rich resources and low cost. Vanadium pentoxide (V_2O_5) is very promising as a host material because of its rich structure, high capacity, easy preparation, and adequate safety. V_2O_5 has several modifications, including α-, β-, δ-, γ-, ζ-, and ε-V_2O_5, as well as hydrate V_2O_5 ($V_2O_5{\cdot}nH_2O$). In this mini-review, we comprehensively summarize the crystal structure of polymorphs V_2O_5 materials, their relationships, and their applications in postlithium batteries, including monovalent (Na^+, K^+), multivalent-ion (Mg^{2+}, Ca^{2+}, Zn^{2+}, Al^{3+}), and nonmetallic (H^+, NH_4^+)-based batteries. Finally, general strategies are reviewed to improve the performance of V_2O_5.

KEYWORDS
crystal structure, energy storage systems, postlithium batteries, strategies, V_2O_5 polymorphs

INTRODUCTION

Renewable energy sources play a crucial role being power supplies to reduce global warming and environmental pollution [1] caused by the large consumption of fossil fuels. In particular, solar and wind power are gradually becoming a large part of the energy proportion share due to the transition to carbon neutrality setting worldwide. However, they are inherently intermittent and generally dispersed, while the consumption and demands of electric energy increase [1e, 2]. Consequently, rechargeable batteries are necessary and essential for large-scale electric energy storage systems (EESs) to realize the smooth integration of these intermittent energies into grids [3].

Lithium-ion batteries (LIBs) have been widely used in portable devices, electric vehicles, and grid storage since their commercialization in the 1990s, because of their high power/energy density, high voltage, and long cycle life [4]. However, their applications on EESs are firmly limited by the manufacturing cost and safety concerns [1e, 5] due to the high cost of raw materials, such as Li_2CO_3, and the low abundance of lithium (only 20 ppm) [6]. Moreover, the unevenly distributed lithium resources (mainly in South America) result in an increased supply chain risk and price. Therefore, it is urgent to develop postlithium batteries based on rich resources and low cost, for example, Na- [4c, 7], K- [8], Mg- [9], Ca- [10], Zn- [11], Al- [12], and nonmetallic (H^+, NH_4^+) [13] batteries.

The reversible intercalation of Li-ions in vanadium pentoxide (V_2O_5) was first reported by Whittingham in 1976 [14] and since then, V_2O_5 has received great attention as cathode material for LIBs. V_2O_5 possesses a layered structure and high capacity (theoretical capacity of 294 mAh g^{-1} with 2 Li^+ ions insertion) and provides high cost-efficiency, easy preparation, and adequate safety [4e, 15]. Moreover, the rich abundance

of vanadium (the 20th most abundant element in the earth's crust) [16] makes it promising for practical application. Besides its application in LIBs, V_2O_5 also has been used as a host for post-Li species, including monovalent (Na^+, K^+), multivalent-ion (Mg^{2+}, Ca^{2+}, Zn^{2+}, Al^{3+}), and nonmetallic (H^+, NH_4^+) [17] owing to large enough interstitial voids in its structure and high capacity (i.e., much higher than that of Prussian blue analogs (PBAs), manganese oxides and organic cathodes). *Note that the term metal-batteries should be used when we consider systems using a metallic anode, while metal-ion (Mg-ion, Ca-ion etc.) batteries should be used when we have a type of "rocking-chair" battery. For the sake of brevity, in this mini-review, we only use the term "metal-ion" batteries*. Considering the significant progress and the versatility of this material, it is necessary to compile and provide to the research community such a review. In this mini-review, we provide a comprehensive introduction of the crystal structure of polymorphs V_2O_5 materials and describe their applications in various "postlithium" batteries. Accordingly, this review is structured as follows: In the first part, the classification of V_2O_5 crystal structure, including α-, β-, δ-, γ-, ζ-, and ε-V_2O_5, as well as hydrate V_2O_5 ($V_2O_5{\cdot}nH_2O$) are reported. In the second part, the progress of V_2O_5 in post-Li batteries is summarized. Finally, in the last section, general strategies used to improve the performance of V_2O_5 are included.

CLASSIFICATION OF V_2O_5 CRYSTAL STRUCTURES

Up to now, several V_2O_5 polymorphs are reported, including α-, β-, δ-, γ-, ζ-, and ε-V_2O_5 as well as hydrate V_2O_5 ($V_2O_5{\cdot}nH_2O$). They crystallize in orthorhombic or monoclinic structures with different space groups because of the different frameworks and arrangements of atoms. Thermodynamically stable phase α-V_2O_5 is the most important and has a close relationship with all other polymorphs that can be obtained via different synthesis approaches using α-V_2O_5 as a starting material. Figure 1 displays the schematic crystal structures of various V_2O_5 polymorphs and their relationship with α-V_2O_5.

α-V_2O_5

The thermodynamically stable polymorph of vanadium pentoxide, α-V_2O_5, is a two-dimensional layered structure, built up from VO_5 square pyramids by sharing edges and corners, where the layers are held together by weak van der Waals forces [18]. It crystallizes in the orthorhombic structure with space group *Pmmn* or $Pmn2_1$, where

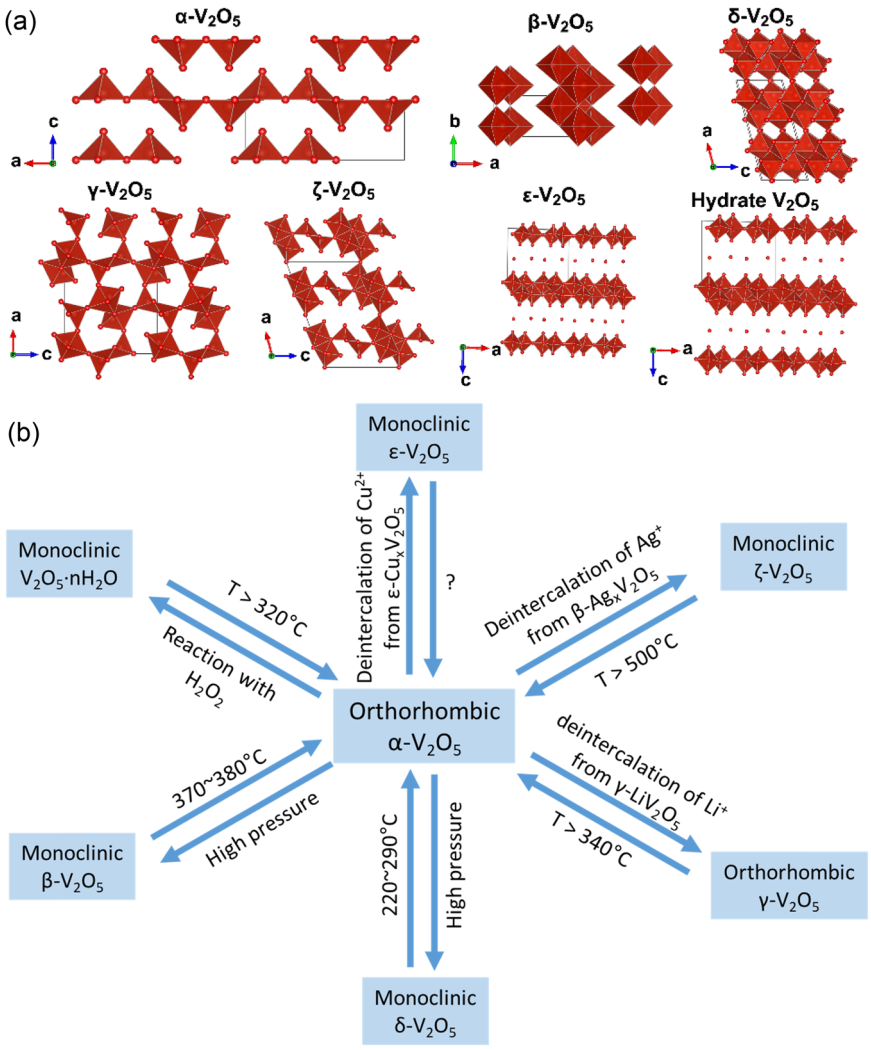

FIGURE 1 Schematic crystal structures (a) of various V_2O_5 polymorphs and their relationship (b) with α-V_2O_5

Pmmn is the common space group [18]. Novák et al. [19] proposed the space group $Pmn2_1$ by studying the single crystal of V_2O_5. $Pmn2_1$ is noncentrosymmetric, while *Pmmn* is centrosymmetric due to the existence of additional inversion symmetry in *Pmmn*. It is impractical to distinguish the two space groups through X-ray powder diffraction analysis, as proved by Novák et al. [19] and Fu et al. [20]. Furthermore, the $[VO_5]$ square pyramids layer of V_2O_5 in space group $Pmn2_1$ is perpendicular to b-axes, while in *Pmmn* it is perpendicular to c-axes. Alternatively, the orthorhombic V_2O_5 structure can be expressed as layers of highly distorted VO_6 octahedra by sharing corners to form a three-dimensional framework.

β-V_2O_5

β-V_2O_5 [21] is a metastable phase prepared at high pressure (6.0 GPa) and V atoms are six-coordinated within distorted VO_6 octahedra. It belongs to the monoclinic structure with a space group $P2_1/m$ and its structure consists of quadruple units of edge-sharing VO_6 octahedra linked by sharing edges along [010] and mutually connected by sharing corners along [001]. This arrangement forms layers of V_4O_{10} composition in planes parallel to (100). The layers are mutually held together by weak forces. β-V_2O_5 is metastable and transforms to α-V_2O_5 at 643–653 K (370–380°C) under ambient pressure.

δ-V_2O_5

δ-V_2O_5 [22] is another metastable polymorph and has very low stability at ambient pressure, which has an isostructure with the B-Nb_2O_5 and Sb_2O_5 and is stable at pressure >8.0 GPa. It also crystallizes in a monoclinic structure but with a space group $C2/c$. The structure can be described as strings of pairs of edge-sharing VO_6 octahedra, which share corners to connect in a zigzag arrangement. The layers formed by strings are stacked parallel to the ac-plane. The δ-V_2O_5 undergoes a phase transformation to α-V_2O_5 in the temperature region 220–290°C in two steps. Both high-pressure phases (β-, δ-) transform into the α-modification when exposed to intense laser radiation [23].

γ-V_2O_5

A metastable variety of vanadium pentoxide is γ-V_2O_5, obtained at atmospheric pressure by chemical or electrochemical deintercalation of Li from γ-LiV_2O_5 as reported by Cocciantelli et al. [24]. γ-V_2O_5 belongs to the orthorhombic structure with space group *Pnma*. The layer structure is built up of puckered layers of edge-sharing distorted VO_5 pyramids. The linkage of the pyramids within the layers is approximately the same as that in γ-LiV_2O_5, but differs from that in the α-V_2O_5 structure. Interestingly, γ-V_2O_5 retains the memory of the original γ-LiV_2O_5 and easily undergoes a phase transformation into α-V_2O_5 upon heating at temperatures higher than 340°C.

ζ-V_2O_5

In contrast to the two-dimensional (2D) layered structure of α-V_2O_5, ζ-V_2O_5 [25] adopts a one-dimensional (1D) tunnel structure based on the hydrothermal deintercalation of Ag^+ ions from nanowires of β-$Ag_xV_2O_5$ tunnel structure. This metastable polymorph crystallizes in a monoclinic structure with space group $C2/m$ and has three distinct distorted VO_6 octahedra and VO_5 square pyramids by sharing edges and corners. These linked chains of polyhedra enclose 1D tunnels along the b-axis with two distinct sites for intercalating cations. The tunnel framework appears to be stable up to 490°C and transforms into α-V_2O_5 only at temperatures >500°C [26].

ε-V_2O_5

ε-V_2O_5 [27] crystallizes in a monoclinic structure with $C2/m$ space group. The coordinates of ε-V_2O_5 were optimized from ε-$Cu_xV_2O_5$ by removing Cu ions since a full structure solution is not available so far. In this structure, distorted $V(1)O_6$ octahedra share edges with an inequivalent set of distorted $V(2)O_6$ and share corners along b- and a-axes to form infinite sheets, which in turn are fused at the edges to form a double-layered structure. The double layers are further connected together via van der Waals force with a larger interlayer spacing than those of α- and ζ-V_2O_5.

Hydrate V_2O_5

Hydrate V_2O_5 ($V_2O_5{\cdot}nH_2O$) [28] is another typical form of vanadium pentoxide and can be obtained through a direct reaction between crystalline V_2O_5 and H_2O_2, which, in turn, can be transformed into orthorhombic V_2O_5 by heat-treatment above 320°C. $V_2O_5{\cdot}nH_2O$ xerogels are composed of V_2O_5 bilayers separated by water molecules, where the double chains are formed by edges and corners sharing VO_6 octahedra. It has a large interplanar spacing of 11.5 Å, where its distance expands or contracts upon guest species (de) intercalation and a distance of about 2.90 Å between the two single V_2O_5 bilayer slabs. The coordination environment of V atoms in each bilayer slab is taken as octahedral.

APPLICATION OF V_2O_5 IN POST-LI BATTERIES

Among these polymorphs, α-V_2O_5 has received the most attention as host materials for Li and post-Li batteries. Herein, we mainly focus on the study of various V_2O_5 in nonaqueous systems for monovalent and multivalent-ion batteries, as shown in Figure 2. Moreover, some

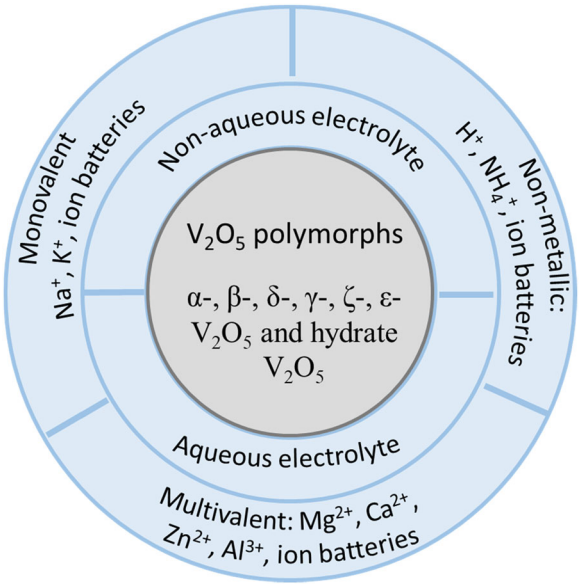

FIGURE 2 Schematic diagram of various post-Li batteries based on V_2O_5 polymorphs

FIGURE 3 Schematic diagram of review order of various V_2O_5 in NIBs. NIBs, Na-ion batteries.

new research findings related to V_2O_5 in aqueous and nonmetallic ion batteries are also summarized.

Na-ion batteries (NIBs)

NIBs, which share a similar working principle as LIBs, have received much attention due to their low cost and abundant resources [3b, 29]. The investigation of NIBs started in parallel with LIBs in the 1970s–1980s [30], but it was then considerably decreased because of the successful commercial application of LIBs in the 1990s. Nowadays, with the increased need to improve the performance of NIBs, it is necessary to explore new electrode materials (cathode and anode), as most of the available cathode materials face structure degradation, low capacity, and slow kinetic diffusion properties owing to the large size of Na^+ ion (1.02 Å of Na^+ vs. 0.76 Å of Li^+) [4d]. Among the polymorphs discussed above, α-V_2O_5 and bilayered V_2O_5 have received the most attention for NIBs due to their high capacity. In this subsection, we will first review the applications of α-V_2O_5 and bilayered V_2O_5 in NIBs (Figure 3). However, V_2O_5 exhibit poor electrochemical performance with limited capacity and cycling stability due to the intrinsic low conductivity of V_2O_5, sluggish diffusion of Na^+, and large volume expansion. Thus, we will also summarize those strategies to address these issues, including the morphology and crystallinity control of V_2O_5, modification of the crystal structure, surface and crystallinity of V_2O_5, and so on. In the end, we will also give an overview about the applications of β-, γ-, and ε-V_2O_5 in NIBs, followed by the studies of V_2O_5 in aqueous NIBs.

α-V_2O_5 was first studied by Jacobsen [31] in 1988 together with channel-type β-$Na_xV_2O_5$ and layered $Na_{1+x}V_3O_8$ in all-solid-state batteries by applying poly(ethylene oxide)-based electrolyte at 80°C. This material demonstrated the insertion of 2 mole of Na^+ insertion during the first discharge and the reversible (de)insertion of 1.7 mole of Na^+ reversible (de)insertion in the following cycles. The formation of a new phase during the first cycle has been observed. In the same year, Pereira-Ramos [32] investigated the electrochemical performance of V_2O_5 in dimethyl sulfone-based molten electrolytes at 150°C for various guest cation insertions, including Na^+, K^+, Cs^+, and Ca^{2+}, which could be inserted with 1.6, 1.2, 0.8, and 0.5 moles per unit, respectively. Interestingly, Dunn et al. [17] in 2004 observed the reversible 1.7-mole insertion of Na^+ into V_2O_5 aerogel in a three-electrode cell configuration, consisting of a carbon paper counter electrode and an Ag wire reference electrode. They also demonstrated the insertion number of various cations, which was up to 1.2 mole of K^+, 0.6 mole of Mg^{2+}, 0.4 mole of Ba^{2+}, per mole V_2O_5 aerogel, respectively. On the other hand, only limited work focuses on the mechanism study of α-V_2O_5 upon Na insertion. Muller-Bouvet et al. [33] reported that upon Na insertion into V_2O_5, the structure of pristine α-phase is maintained in $x \leq 0.2$ in $Na_xV_2O_5$ and proceeds via a solid solution mechanism in the range $0.2 \leq x \leq 1.6$. The irreversible NaV_2O_5 phase is formed during the first Na insertion and the NaV_2O_5 phase can reversibly insert 0.8 sodium ions in the potential range of 1.4–3.0 V versus Na^+/Na. However, Ali and coworkers [34] proposed a different reaction mechanism. A two-phase mixture composed of a major phase NaV_2O_5 and a minor phase $Na_2V_2O_5$ was observed during the discharge process. According to Ali et al., upon charging, the material returns back to its original structure of V_2O_5 with a minor phase of NaV_2O_5.

To improve the capacity and cycling stability of V_2O_5, amorphous V_2O_5 was prepared, which demonstrated two times the higher specific capacity of 241 mAh g^{-1} than the crystalline one (120 mAh g^{-1}), as well as a high discharge potential, high energy density, and long cycle stability [35]. Differently, Liu et al. reported that amorphous V_2O_5 can provide higher reversible capacities than the crystalline one at low current densities, but not at high current densities (>320 mA g^{-1}) [36]. The encapsulated V_2O_5/nanoporous carbon nanocomposite exhibits a capacity of 170 mAh g^{-1} at 40 mA g^{-1} and high-rate performance with a capacity of 90 mAh g^{-1} at 640 mA g^{-1} [37]. Porous hollow spherical α-V_2O_5 with exposed (110) facets delivers a specific discharge capacity of 150 mAh g^{-1} at 20 mA g^{-1} and good cycling performance [38]. V_2O_5 microspheres [39], thin film [40], V_2O_5/TiO_2 [41], nanocomposite [42], were also studied.

Nanostructured $V_2O_5{\cdot}nH_2O$ with different interplanar spacings [43] were prepared and applied as electrode materials in NIBs. In addition, cation preinsertion such as Fe- [44], K- [45], Na- [46],

Mn- [47], NH_4^+ [48] preintercalated $V_2O_5{\cdot}nH_2O$, graphene oxide/$V_2O_5{\cdot}nH_2O$ [49] composites were also introduced to improve the performance of $V_2O_5{\cdot}nH_2O$. For example, electrochemically deposited nanostructured $V_2O_5{\cdot}nH_2O$ has an interplanar spacing of ~13.5 Å and achieves a reversible capacity of 250 mAh g^{-1} at 20 mA g^{-1} with average potentials of 3 V in NIBs [43a]. Single-crystalline $V_2O_5{\cdot}nH_2O$ nanobelts via the solvothermal method have a large interlayer spacing of ~11.53 Å with a thickness of ~50 nm. The material exhibits a high capacity of 231.4 mA h g^{-1} at 80 mA g^{-1} with the formation of $Na_2V_2O_5$ (expanded interlayer spacing of 15.35 Å) [43b]. V_2O_5 aerogel was applied as an anode and delivers a capacity of 200 mAh g^{-1} in the voltage range 0.01–1.5 V versus Na^+/Na. Furthermore, the material was coupled with a carbon-coated $Na_3V_2(PO_4)_3$ cathode to build a full Na-ion cell, showing an average voltage of 2.5 V [43e]. $V_2O_5{\cdot}nH_2O$ nanoflakes grown on a three-dimensional (3D) stainless steel mesh substrate display excellent electrochemical performance for Li-, Na-, and Al-ion intercalation, with a stable capacity of 250, 110, and 80 mA h g^{-1} after 100 cycles for Li-, Na-, and Al-ion batteries, respectively (Figure 4) [43j]. Bilayered $Na_xV_2O_5{\cdot}nH_2O$ nanowires were synthesized and demonstrated a high initial discharge capacity of 365 mAh g^{-1} at 20 mA g^{-1} (1.0–4.3 V vs. Na/Na^+) [50].

The layered β-V_2O_5 modification was investigated for NIBs by Córdoba et al. [51] and exhibits an initial discharge capacity of 132 mAh g^{-1} with multiple clear plateaus above 2.4 V at C/20 and a maximum capacity of 147 mAh g^{-1} (1-mole Na^+ ion insertion) under equilibrium conditions. They claimed the appearance of several isostructure $Na_xV_2O_5$ ($0 \le x \le 1$) by ex situ X-ray powder diffraction (XRD) and the irreversible phase transformation after the full Na^+ extraction. The same group also studied the impact of partial fluorine substitution on monoclinic β-$Na_{0.33}V_2O_5$ by both theoretical and experimental methods. The oxyfluoride β-$Na_{0.33}V_2O_{4.67}F_{0.33}$ shows the same structure as that of β-$Na_{0.33}V_2O_5$ with space group *A*2/*m*, but significant changes in sodium environment (shortening of the Na-anion bond lengths) [52]. However, β-$Na_{0.33}V_2O_{4.67}F_{0.33}$ displays a less capacity than that of β-$Na_{0.33}V_2O_5$ owing to its lower diffusion coefficient, less adequate morphology, and a lower oxidation state of vanadium originating from aliovalent O/F substitution. γ-V_2O_5 was applied as a new Na-ion insertion cathode material for NIBs, which was prepared by a chemical reaction between γ-LiV_2O_5 and NO_2BF_4 oxidizing agent [53]. γ-V_2O_5 displays a flat plateau at 3.3 V with a maximum specific capacity of 145 mAh g^{-1} (1 Na^+ insertion). The material suffers from a strong kinetic limitation, as proven by the low efficiency at room temperature (RT) and high efficiency at 50°C.

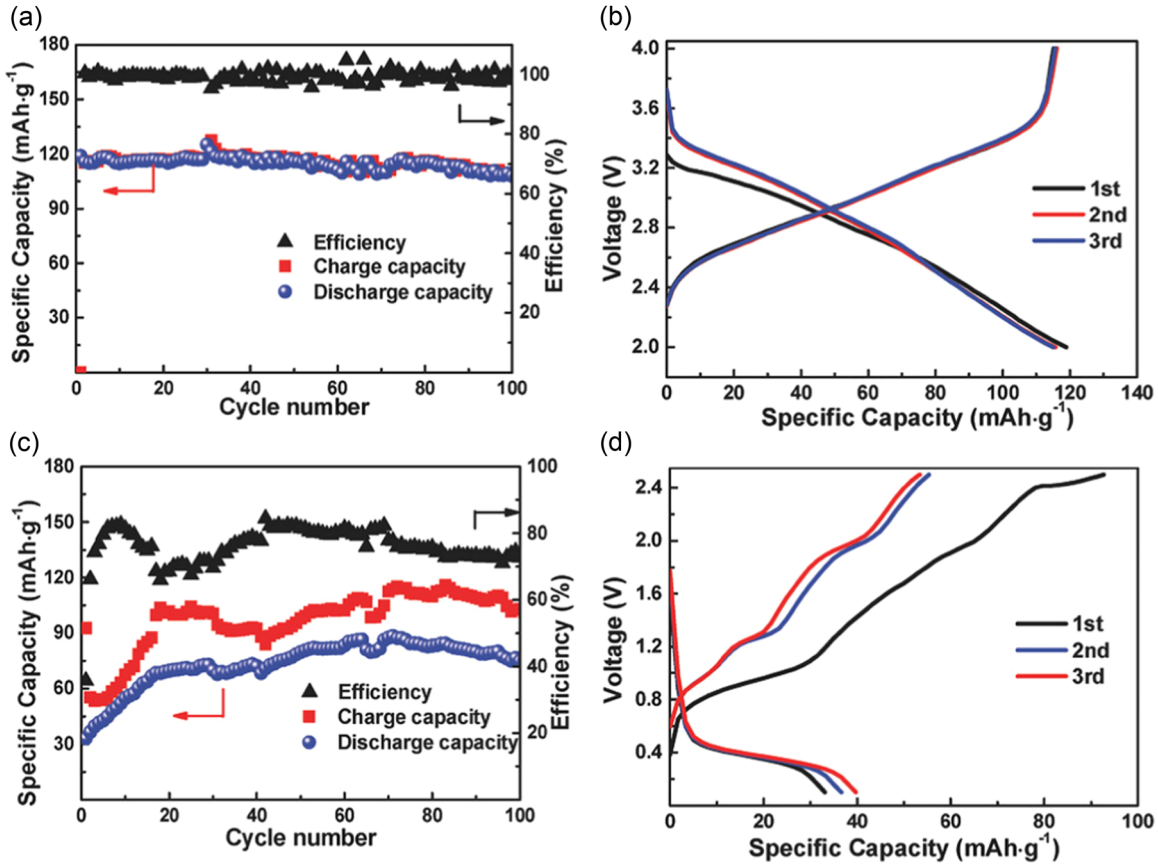

FIGURE 4 Cycle performance and discharge-charge profiles of $V_2O_5{\cdot}nH_2O$ in Na-ion batteries (a, b) and Al-ion batteries (c, d) at 100 mA g^{-1}. Reproduced with permission from Wang et al. [43j], Copyright 2017 Wiley-VCH.

γ-V_2O_5 undergoes a two-phase transition involving the formation of a new phase γ-$Na_{0.7}V_2O_5$ followed by a solid solution. Due to its zero strain, γ-$Na_xV_2O_5$ structure also has remarkable cycling stability [53]. The structural changes upon sodiation are highly correlated to the evolution of cathode impedance, diffusion coefficient, and charge transfer [54]. Compared with the as-synthesized γ-V_2O_5, ball-milled γ-V_2O_5 demonstrates smaller particles, an increased charge efficiency of 90% from 50%, and an enhanced discharge capacity of 120 mAh g^{-1} at C/2 [55]. Later on, the crystal structure of the electrochemically synthesized γ-$Na_{0.97}V_2O_5$ was solved by Rietveld refinement and Raman spectroscopy, showing an orthorhombic layered structure (*Pnma* space group) with Na ions occupied the large octahedral sites between interlayer [56]. Then, high crystallinity γ-$Na_{0.97}V_2O_5$ was synthesized by chemical reaction using γ-V_2O_5 and NaI in acetonitrile at RT. The cathode material demonstrates an initial specific capacity of 125 mAh g^{-1} at C/5 and 112 mAh g^{-1} after 50 cycles [57]. ε-V_2O_5 and γ-V_2O_5 materials possess a high average voltage of 2.8 V in NIBs, which is 1 V higher than α-V_2O_5 and related to their unique open frameworks that result in higher chemical potentials [58]. ε-V_2O_5 delivers a much higher capacity (200 mAh g^{-1}) than that of γ-V_2O_5 (120 mAh g^{-1}) at C/10, where the electrodes using carbon nanotubes (CNTs) conductive agent exhibit a much-improved capacity and rate capability compared with that using carbon black/graphite (AB/graphite) [59].

In addition, graphene-modified vanadium pentoxide (V_2O_5@G) was applied as electrode material in aqueous NIBs, which was coupled with a high-voltage cathode $Na_{0.44}MnO_2$ to assemble a full cell. However, the electrode delivers limited charge–discharge capacity (38 mAh g^{-1}) and cyclic stability with a retention of 53% after 200 cycles at 1 A g^{-1} [60]. $V_2O_5{\cdot}0.6H_2O$ nanoribbons were investigated in aqueous electrolyte solutions of 0.5 M Li_2SO_4, Na_2SO_4, and K_2SO_4, providing a reversible capacity of 37, 43, and 50 mAh g^{-1} at 100 mA g^{-1}. Interestingly, the material shows the most capacity and facile K^+ insertion, despite its highest ionic radius among the three cations (Li^+, Na^+, and K^+) [61].

At present, NIBs are a very promising technology and alternative to LIBs due to the advantages of abundant resources and the low cost of the related raw materials. Particularly, the breakthrough of commercial NIBs made by contemporary amperex technology co. limited (CATL), consisting of Prussian white cathode and porous structure hard carbon anode, brings light to the world [62]. The battery developed by CATL provides a high energy density of 160 Wh kg^{-1} and fast charge to 80% state of charge (SOC) in 15 min [62], which is comparable with that of commercial $LiFePO_4$ (90–160 Wh kg^{-1}). This further encourages researchers and scientists to put more effort into developing advanced electrode materials with high capacity and cycling stability. It is well-known that analogs electrode materials in NIBs behave significantly differently than in LIBs. Still, NIBs face the issues that few electrode materials can reversibly (de)insert Na^+ ions with fast kinetics and good cycling stability because of the large size of Na^+ ions. Vanadium oxide has a much higher capacity than that of commercial Prussian white (150 mAh g^{-1}) and is very promising for the application in NIBs, in particular, given its large interlayer spacing, which can minimize the volume expansion and increase the diffusion kinetics upon cycling. However, as a general hint to researchers in this field, careful attention should be paid during the electrochemical study of electrode materials to the usage of the highly reactive metallic Na in ether-based electrolytes [63]. In summary, much work still needs to be done in the development of advanced vanadium oxide electrode materials before their practical application in NIBs.

Potassium-ion batteries (KIBs)

Eftekhari [64] designed the first rechargeable KIB in 2004 by employing Prussian blue and potassium metal with 1 M KBF_4 in a carbonate-based electrolyte, where KIBs share a similar working principle ("rocking chair") as that of LIBs. However, KIBs did not receive much attention until Kim et al. [65] reported the electrochemical activity of an amorphous $FePO_4$ cathode in 2014. Afterward, KIBs received much interest as a promising candidate for the large-scale EESs due to the abundance and low cost of potassium. Although K-ion is larger and heavier than Li^+, Na^+, and Mg^{2+}, the K^+/K couple has a lower standard electrode potential (−2.936 V vs. SHE) than that of Na^+/Na (−2.714 V vs. SHE) and Mg^{2+}/Mg (−2.37 V vs. SHE) [27b, 66].

Pereira-Ramos [32] in 1988 investigated the electrochemical performance of V_2O_5 in dimethyl sulfone-based molten electrolytes at 150°C for various guest cation insertions, including Na^+, K^+, Cs^+, and Ca^{2+}, 1.6, 1.2, 0.8, and 0.5 moles per unit, respectively. The first application of V_2O_5 at RT as a host for K-ion insertion dates back to 2004 when Dunn et al. [17] realized the reversible insertion of Na^+, K^+, Mg^{2+}, and Ba^{2+} applying V_2O_5 aerogel in a three-electrode cell, consisting of carbon paper counter electrode and Ag wire reference (RE). They demonstrated the insertion number of various cations up to 1.7 moles of Na^+, 1.2 moles of K^+, 0.6 moles of Mg^{2+}, 0.4 moles of Ba^{2+}, per mole V_2O_5 aerogel, respectively. Huang et al. [67] prepared a core-shell structured V_2O_5@CNT sponge that is able to offer fast ion insertion/deinsertion with a high capacity of 206 mAh g^{-1} at 5 mA g^{-1}. V_2O_5 nanorod@rGO [68] shows a higher reversible capacity of 271 mAh g^{-1} at 29.4 mA g^{-1} and good cycling stability of 80% after 500 cycles. The potassium storage mechanism in orthorhombic V_2O_5 nanoparticles was studied in our previous work [20] *via* in operando synchrotron diffraction and XAS. However, in that work, V_2O_5 nanoparticles suffered from a fast and severe capacity fading from 200 to 54 mAh g^{-1} followed by a slight and slow increase to 80 mAh g^{-1} after 200 cycles. Moreover, a "cathode electrolyte interphase" (CEI) formation/decomposition was revealed during the first cycle. First-principles calculations demonstrated that a monolayer of V_2O_5 has a much smaller migration barrier for Na^+ and K^+ (0.44 and 0.39 eV) than bulk V_2O_5 (1.66 eV) [69], demonstrating that bulk V_2O_5 is not suitable for Na-, K-, and Mg-ion batteries because of high migration barriers. Moreover, Manzhos et al. [70] demonstrated that metastable β-V_2O_5 offers much smaller diffusion barriers compared with orthorhombic α-V_2O_5 for K-ion insertion.

Compared with α-V_2O_5, layered γ-V_2O_5 polymorph shows a flat plateau at the high potential of 3.3 V versus K^+/K and limited initial depotassiation capacity of 72 mA h g^{-1} at C/10 as reported by Pereira-Ramos et al. [71]. γ-V_2O_5 undergoes a two-phase transition to form $K_{0.5}V_2O_5$ (space group *Pnma*), followed by a solid solution with the formation of $K_{0.78}V_2O_5$ during the first discharge. In the following cycles, the material displays reversible depotassiation–potassiation within $K_xV_2O_5$ ($0.3 \le x \le 0.78$) and less than 2% volume variation.

K^+ preintercalation is a strategy adopted to overcome the challenges of relatively low capacity and unsatisfactory cycling stability. Indeed, K^+ preintercalcated V_2O_5 materials ($K_{0.83}V_2O_5$ [72], $K_{0.5}V_2O_5$ [73], δ-$K_{0.51}V_2O_5$ [74], $K_{0.486}V_2O_5$ [75], $K_{0.23}V_2O_5$ [76]) are supposed to have improved performance with respect to V_2O_5. One example is a layered and moisture nonsensitive $K_{0.83}V_2O_5$ (space group *Pnma*), which was reported by Zhu et al. [72]. $K_{0.83}V_2O_5$ displays an initial potassiation capacity of 90 mAh g^{-1} with a plateau at 3.5 V and capacity retention of 88% after 90 cycles. DFT calculation shows that $K_xV_2O_5$ ($0 < x \le 0.875$) displays a (semi)metallic feature upon potassiation and one-dimensional K-ion transport path. Jiang and coworkers [74] prepared single-crystalline bilayered δ-$K_{0.51}V_2O_5$ nanobelts (KVOs) via reorganization of α-V_2O_5, which shows a high average voltage (3.2 V), high capacity (131 mAh g^{-1}), and good rate capability even at 10 A g^{-1} (Figure 5). They also found that the excellent K-ion storage performance of KVO is due to the large interlayered structure and unique 1D morphology by combining experiments with theoretical calculations. Xie et al. [75] synthesized K^+ preintercalated $K_{0.486}V_2O_5$ (interplanar spacing of 9.4 Å) nanobelts. $K_{0.486}V_2O_5$ cathode displays a high capacity of 159 mAh g^{-1} at 20 mA g^{-1} with a capacity retention of 67.4% after 100 cycles at 100 mA g^{-1}, which is ascribed to the lower diffusion barriers and shorter diffusion distances in comparison to α-V_2O_5 [74].

Hydrate V_2O_5 ($V_2O_5{\cdot}nH_2O$) is very promising as a cathode as its large interplanar spacing is >11 Å. Li et al. [77] synthesized a reticular $V_2O_5{\cdot}0.6H_2O$ with a large interplanar spacing of 13.3 Å, which delivers an initial discharge capacity of 224 mAh g^{-1} with capacity retention of 46% after 500 cycles at 50 mA g^{-1}. The material exhibits improved electrochemical activity because of the enlarged layer space compared with crystalline α-V_2O_5. $V_2O_5{\cdot}0.8H_2O$@GO material displays good cycling stability (94% after 200 cycles at 500 m Ag^{-1})

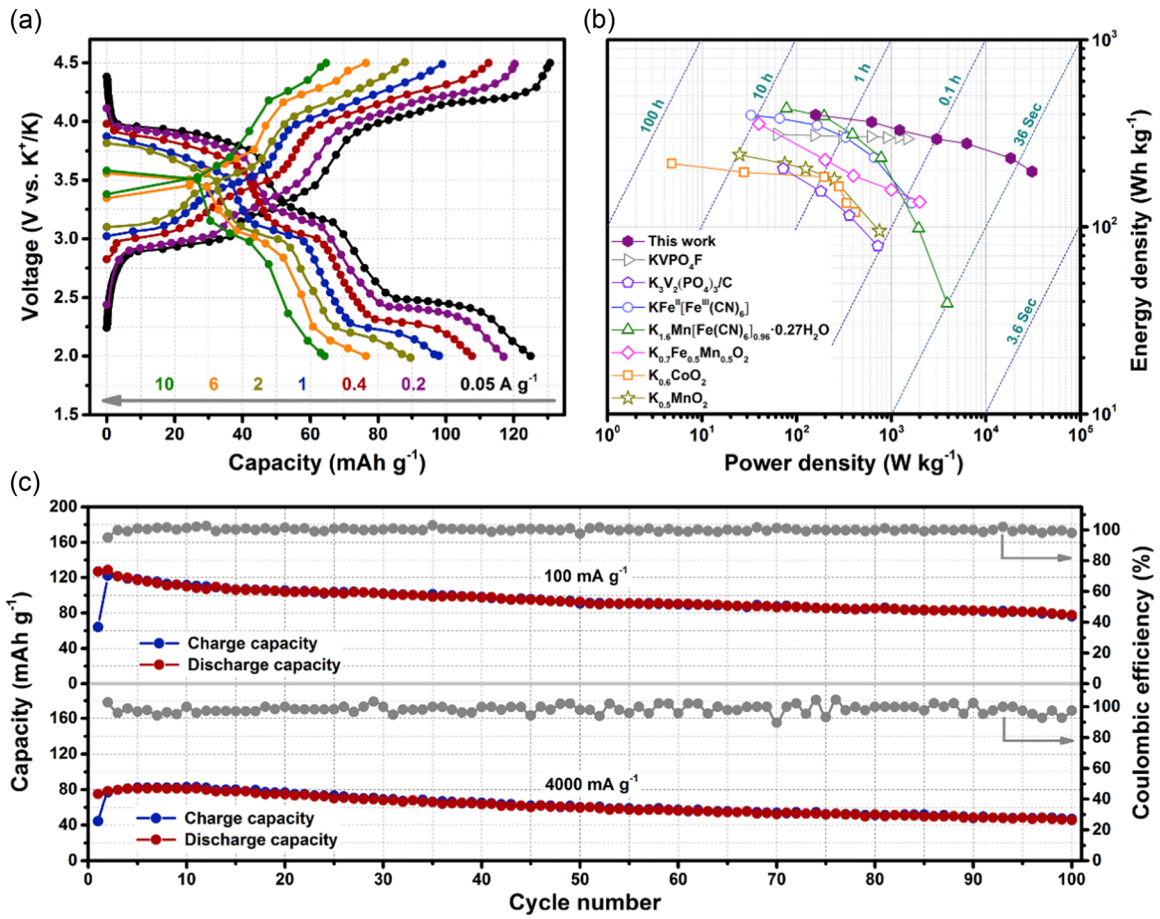

FIGURE 5 Charge-discharge profiles of the KVO electrodes at different current densities (a), Ragone plots of the KVO cathode and other advanced potassium-ion battery cathodes (b), and cycle performance (c) of the KVO electrodes at 100 and 4000 mA g^{-1}. Reproduced with permission [74], Copyright 2019 Elsevier.

but low reversible capacities of 93 mAh g^{-1} at 50 m Ag^{-1} as reported by Passerini et al. [78], who demonstrated that a highly concentrated potassium bis(trifluoromethanesulfonyl)imide-glyme electrolyte effectively suppresses the decomposition of the electrolyte solvent and dissolution of Al current collector. δ-$K_{0.42}V_2O_5$·0.25H_2O [79], $K_{0.5}V_2O_5$·0.5H_2O [73c], and $Na_{0.29}V_2O_5$·$n$$H_2O$/rGO/CNT composites [80] are also reported as cathode for KIBs. Interestingly, δ-$K_{0.42}V_2O_5$·0.25H_2O with an interlayer spacing of 9.65 Å shows an initial discharge capacity of 268 mAh g^{-1} at C/50 and 226 mAh g^{-1} at C/15 with capacity retention of 74% after 50 cycles, which is much higher than that of $Na_{0.29}V_2O_5$·$n$$H_2O$/rGO/CNT (interplanar spacing of 11 Å, 120 mAh g^{-1} at 0.1 A g^{-1}).

Moreover, aqueous KIBs based on V_2O_5 are also reported. For example, Teng et al. [81] reported a polymer pre-intercalated V_2O_5 (polymer molecule in the interlayer) with an increased interlayer distance of 22 Å for aqueous KIBs, which shows high capacities of 126, 114, and 91.0 mAh g^{-1} in 1 M KCl at the current densities of 50, 100, and 200 mA g^{-1} after 100 cycles, respectively. Later on, the same group [82] synthesized disordered vanadium oxide nanosheets $K_{0.22}V_{1.74}O_{4.37}$·0.82H_2O for aqueous KIBs. This material delivers a high capacity of 183 mAh g^{-1} and excellent cycle stability in KCl electrolyte; its good performance is attributed to the crystal water and structural reorganization. Interestingly, Jiang et al. [83] reported an aqueous K-ion microbatteries, consisting of amorphous/crystalline dual-phase $K_xV_2O_5$·$n$$H_2O$ anode and K_xMnO_2·$n$$H_2O$ cathode in aqueous 0.5 M K_2SO_4. The resulting full microbattery delivers a maximum energy density of 103 mWh cm^{-3} and maximum power densities of ~600 W cm^{-3}, which is comparable with carbon-based microsupercapacitors.

Nowadays, KIBs are still at their beginning stages due to the lack of suitable host materials with satisfactory electrochemical performance. Insertion materials often suffer from sluggish K^+ diffusion kinetics and irreversible structural transformation arising mostly from the large size of K^+ during cycling. Fortunately, considerable progress has been made with regard to the development of anodes for PIBs. Carbon-based materials deliver high capacities (≥250 mAh g^{-1}) with good cycling stability [8]. However, the capacity of most cathode materials is still unsatisfactory (~150 mAh g^{-1}). V_2O_5 polymorphs can deliver a higher capacity of ~250 mAh g^{-1} but still suffer from poor rate capability, cycling stability, and phase transitions owing to the large ionic size of K^+. Further engineering of vanadium oxides is needed to provide sufficient storage sites and diffusion channels for the large K-ions, and the in-depth reaction mechanisms need to be clarified. For full-cell configurations, V_2O_5 can be coupled with presodiated hard carbon in NIBs and prepotassiated graphite in KIBs, while V_2O_5 can be coupled with Na/K metal in half-cell configurations for NIBs and KIBs. The problems are arising in half-cell configurations due to the highly reactive K metal and side reaction of electrode/K metal (similar to Na). Therefore, special attention should be paid to the electrode/electrolyte interphase and electrolyte engineering to reduce side reactions and improve the overall performance of KIB (NIBs) half cells.

Magnesium-ion batteries (MIBs)

MIBs are considered a promising candidate for large-scale EESs since they offer high safety, low cost, and high volumetric capacity (3833 mAh cm^{-3}). The first Mg rechargeable battery system was proposed by Gregory et al. [84] in 1990, consisting of an electrolyte containing Mg-organo-borate moieties, $Mg(BBu_2Ph_2)_2$, in tetrahydrofuran (THF). The electrolyte allows reversible Mg deposition/dissolution with an electrochemical stability window of <2 V, while it is incompatible with transition metal oxides or sulfides. Ten years later, Aurbach et al. [85] made the second breakthrough in this field and developed the first rechargeable magnesium battery consisting of Mg metal, Chevrel phase cathode, and $Mg(AlCl_2BuEt)_2$ electrolyte. Then a new all-phenyl-complex (APC) electrolyte with a wide electrochemical window (>3 V) was developed by the same group [86]. Despite these breakthroughs, one of the major issues faced by MIBs is the lack of high-performance cathode materials and the lack of an electrolyte that is simultaneously compatible with high-voltage cathodes and the Mg anode [87]. In addition, the most common Mg-ion electrolytes exhibit high corrosion to the battery casing and current collectors. For instance, stainless steel becomes unstable above 2 V versus Mg^{2+}/Mg in the well-known APC electrolyte [88].

The magnesiation behavior of α-V_2O_5 through either electrochemical or chemical intercalation was first studied in 1980s [89] and 1990s [84, 90] despite the development of $Mg(BBu_2Ph_2)_2$/THF electrolyte. These pioneering efforts demonstrate the promising aspects of V_2O_5 due to its high OCV (2.66 V) and modest capacity of 196 mA h g^{-1}. V_2O_5 can reversibly (de)intercalate Mg^{2+} ions, while no electrolyte is available that is compatible with both V_2O_5 and Mg. Aurbach et al. [91] studied the reversible Mg (de)intercalation of thin V_2O_5 film in nonaqueous Mg salt solutions using activated carbon (AC) as both counter electrode (CE) and RE (Figure 6). The V_2O_5 electrode exhibits reversible Mg-ion intercalation with capacities around 150–180 mAh g^{-1}. The rational design of electrode materials is an effective method to improve their electrochemical performance, such as preparing nanostructured materials, heterogeneous structures (including surface coating, composites), and cation doping.

Spherical V_2O_5 with a hierarchical architecture was proven to deliver a high capacity of 225 mA h g^{-1} at 10 mA g^{-1}, which stabilized at ≈190 mA h g^{-1}; the V_2O_5 material remains in its phase and morphology after cycling [92]. Zhao et al. [93] designed a dual-functional V_2O_5 with a honeycomb-like structure and rich oxygen vacancies with the aim to improve electronic conductivity and diffusion kinetics. They proved that Mg^{2+} intercalation occurs from the (101) plane of V_2O_{5-x}. Amorphous V_2O_5 [94], V_2O_5–P_2O_5 [95], GO/V_2O_5 [96], and V_2O_5/S [97] composites are also prepared to improve the capacity and cycling stability of V_2O_5. For instance, V_2O_5/S composite displays a much higher capacity (310 mAh g^{-1}) than that of pristine V_2O_5 (160 mAh g^{-1}). Manzhos et al. [98] calculated the interaction mechanism of α-V_2O_5, β-V_2O_5, VO_2(R), and VO_2(B) upon Li^+, Na^+, Mg^{2+}, and Al^{3+} insertion, where rutile VO_2(R) holds the largest binding energy and a low diffusion barrier

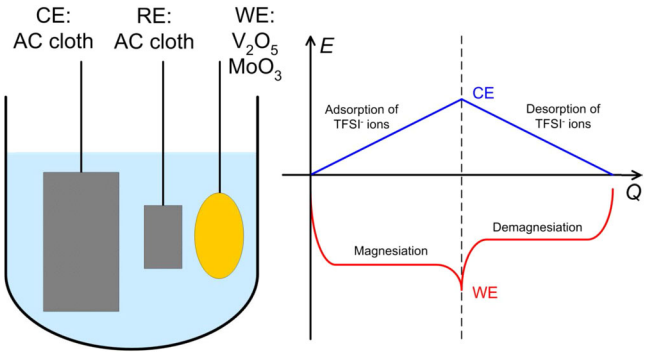

FIGURE 6 Scheme of the cell configuration and the electrode processes. AC cloth was used as RE and CE. The charge passage needed for the magnesiation/demagnesiation processes of the working electrode (CE, V_2O_5) is maintained by non-Faradaic, electrochemical adsorption/desorption on the high surface area CE (interfacial capacitance). The potential (E) of the CE is linear with the charge (Q), with a slope of 1/C, where C is the capacitance of CE. Reproduced with permission from Gershinsky et al. [91]. Copyright 2013 American Chemical Society. AC, activated carbon; CE, counter electrode; RE, counter electrode.

for Al^{3+} and β-V_2O_5 displays the highest binding energy and reduced diffusion barrier for Mg^{2+} compared to α-V_2O_5. $NH_4V_4O_{10}$ [99] and Zr^{4+}-doped $NH_4V_4O_{10}$ [100] present an improved discharge capacity and cycling stability due to the expanded interlayer space.

Water in electrolytes plays an important role in achieving high capacity. Yu and Zhang [101] reported that V_2O_5 displays the highest first discharge specific capacity of 159 mAh g^{-1} in 0.1 M $Mg(ClO_4)_2$ + 1.79 M H_2O/PC among various electrolytes, as water can facilitate the electrochemical Mg^{2+} (de)intercalation. Sa et al. [102] studied the compatibility of $Mg(TFSI)_2$/diglyme electrolyte with Mg metal and α-V_2O_5 at very low water levels. They found that electrolytes containing high-level water cannot reversibly deposit Mg, but contributes to higher capacities, which originate from the reversible proton insertion. On the other hand, it is critical to reduce the water amount in the $Mg(TFSI)_2$/diglyme electrolyte to obtain reversible Mg plating/stripping. Hong et al. [103] reported that the crystal structure of magnesiated α-V_2O_5 has a general formula of $Mg_{0.17}H_xV_2O_5$, ($0.66 \le x \le 1.16$) in 0.5 M $Mg(ClO_4)_2$/AN + 2.0 M H_2O and found that single Mg^{2+} ions or protons are the only intercalated ions since H_2O, H_3O^+, or solvated magnesium ions are too big for the cavities. Palacín et al. [104] demonstrated the formation of H^+ inserted V_2O_5 with negligible Mg^{2+}/Ca^{2+} content in both dry and wet carbonate-based electrolytes at RT and 100°C and the formation of orthorhombic phase caused by degradation via both water and temperature. α-V_2O_5 is traditionally regarded as a promising host to reversibly uptake high content of Mg^{2+}, while it is reported that H^+ intercalation dominates the observed electrochemical activity rather than Mg^{2+}. To address this controversy, Yoo et al. [105] performed electrochemical tests using chemically and anodically stable ionic liquid electrolyte at 110°C and found that the layered α-V_2O_5 reversibly deliver capacities above 280 mAh g^{-1} with 1 mol Mg^{2+} intercalation per unit formula. Aurbach et al. [106] studied the effect of DME on the Mg^{2+} intercalation kinetic into thin V_2O_5 films in $Mg(ClO_4)_2$/AN electrolyte. They found that DME-Mg interaction forms stable solution structures that kinetically slow down the insertion of the Mg^{2+} cations into V_2O_5 since DME forms a more stable 3DME-Mg^{2+} solvated structure by replacing the ACN-Mg^{2+} cation. Mukherjee et al. [107] demonstrated the phase formation from α-V_2O_5 to ε-$Mg_{0.5}V_2O_5$, which is different from the chemically synthesized sample of δ-MgV_2O_5. In our previous work [88], we clarified the reaction mechanism of α-V_2O_5 via in operando synchrotron diffraction and X-ray absorption spectroscopy by applying a full cell configuration, consisting of α-V_2O_5 cathode $Mg_xMo_6S_8$ ($x \approx 2$) anode and 1 M $Mg(ClO_4)_2$/AN electrolyte. α-V_2O_5 undergoes a two-phase transition with the formation of ε-$Mg_{0.6}V_2O_5$ phase (Figure 7).

Metastable ζ-V_2O_5 was first used as Mg^{2+} insertion host by Banerjee et al. [108], which holds up to 0.33 mol Mg^{2+} per V_2O_5 with a capacity of 90 mAh g^{-1} after 100 cycles. However, ζ-V_2O_5 suffers from poor Mg^{2+} kinetics and large voltage hysteresis, Darr et al. [109] improved the discharge capacity of ζ-V_2O_5 to 130 mAh g^{-1} with low voltage hysteresis of 1.0 V by synthesizing nanosized (ca. 100 nm) ζ-V_2O_5. Cabana et al. [110] investigated the role of H_2O in ionic liquid electrolytes using tunnel ζ-V_2O_5, where H_2O concentration closely influences the electrochemical reaction and V reduction, but not on changes in cell volume and Mg content. They concluded that H_2O raises competing pathways rather than enhancing Mg^{2+} intercalation, suggesting that the addition of H_2O into electrolytes is not a universal solution to improve Mg^{2+} intercalation for oxides.

Interplanar spacing expansion of V_2O_5 is believed to be an effective approach to improve ion diffusions, such as using water crystal water [111] and/or cations or polymer/composites [112]. Smyrl et al. [113] demonstrated that V_2O_5 aerogel can hold polyvalent cations such as Mg^{2+}, Al^{3+}, and Zn^{2+} inside the host via chemical intercalation, which has up to 4 mol of Mg^{2+}, 3.33 mol of Al^{3+} 2.5 mol of Zn^{2+}, per mol V_2O_5 aerogel, respectively. V_2O_5 xerogel/carbon composites [114] show 1.84 mol of Mg^{2+} intercalation per mol of V_2O_5 at 0.1 mV s^{-1}, corresponding to a capacity of 540 mAh g^{-1}, which is much higher than that of V_2O_5 xerogel (150 mAh g^{-1}). The Mg^{2+} intercalation of V_2O_5 xerogel/carbon composites shows two main broad peaks similar to that of Li^+, where the first and second peaks are related to Mg^{2+} intercalated into innerlayer site of V_2O_5 and interlayer site, respectively [115]. Yao et al. [111b] fabricated V_2O_5·1.42H_2O@rGO nanocomposite, which delivers a capacity of 330 mAh g^{-1} at 50 mA g^{-1} and displays high capacity retention of 81% after 200 cycles at 1 A g^{-1}. Moreover, the material works well in a wide temperature range of [−30°C, 55°C] with a capacity higher than 200 mAh g^{-1} at 55°C. Ceder et al. [116] calculated and H_2O-Mg^{2+} cointercalation into V_2O_5 Xerogel and revealed the important role of H_2O during intercalation, where H_2O-Mg^{2+} cointercalation in wet electrolytes results in higher voltages compared with that obtained with dry electrolytes. Sa et al. [117] proved Mg^{2+}-diglyme cointercalation into V_2O_5·nH_2O using NMR, where V_2O_5·nH_2O shows contraction/expansion upon Mg intercalation/deintercalation because of the strong electrostatic interaction

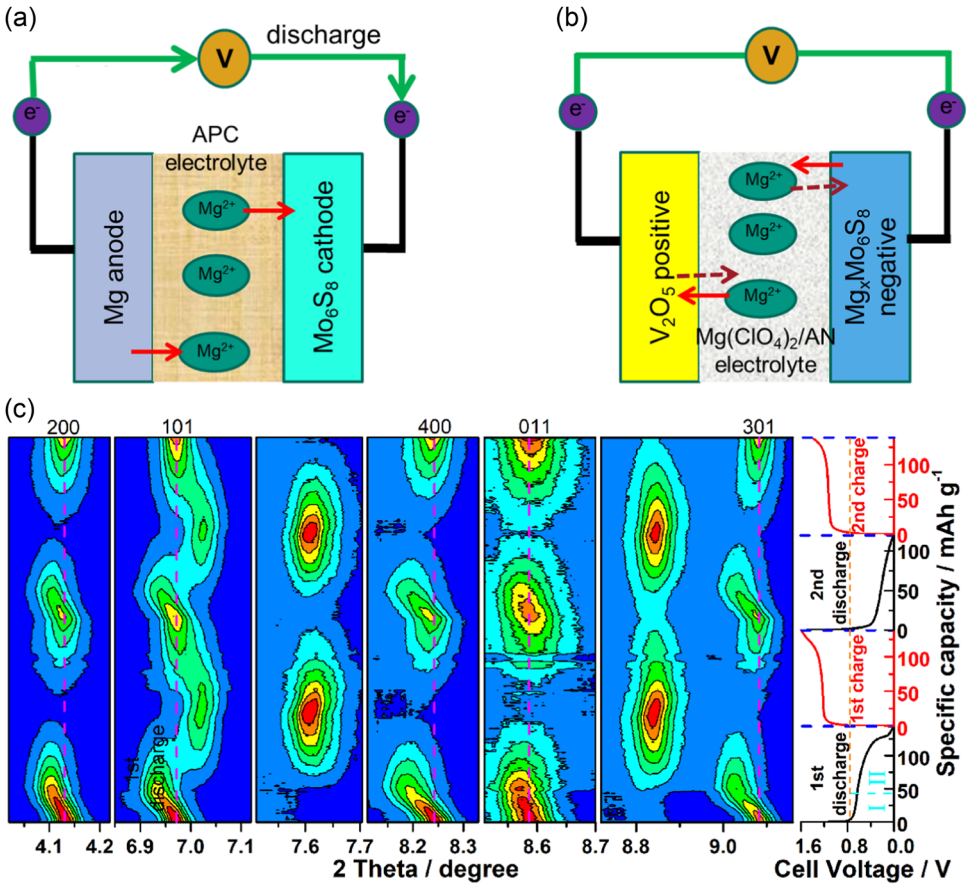

FIGURE 7 Scheme of the half-cell for the electrochemical preparation of the $Mg_xMo_6S_8$ anode (a), V_2O_5 | $Mg(ClO_4)_2$/AN | $Mg_xMo_6S_8$ ($x \approx 2$) cell configuration (b), and Contour maps of in operando synchrotron diffraction of V_2O_5 collected during the first two cycles at C/25 (c). Reproduced with permission [88]. Copyright 2019 American Chemical Society.

between Mg^{2+} and $V_2O_5{\cdot}nH_2O$. Mn^{2+} and Mg^{2+} preintercalated hydrated vanadium oxides [118] exhibit excellent rate performance and cycling stability, where crystal water inside the structure enables fast Mg^{2+} ions mobility because of its charge shielding effect and pre-intercalated Mn^{2+}/Mg^{2+} cations lead to high electronic conductivity and structural stability.

In addition, V_2O_5 nanowires exhibit a high discharge capacity of 359 mAh g^{-1} with capacity retention of 80% after 100 cycles in aqueous Mg-ion batteries, as demonstrated by Fu et al. [119], who designed a highly safe aqueous Mg-ion electrolyte with a wide electrochemical stability window of 3.7 V, consisting of polyethylene glycol and 0.8 m $Mg(TFSI)_2$. The authors also revealed two 2-phase transition processes with the formation of ε-$Mg_{0.6}V_2O_5$ and Mg-rich $Mg_xV_2O_5$ ($x \approx 1.0$) and CEI containing MgF_2 as the major component in aqueous Mg-ion batteries. Xu and coworkers [120] developed a tetraethylene glycol dimethyl ether (TEGDME) – water hybrid electrolyte with an electrochemical stability window of 3.9 V. $NaV_8O_{20}{\cdot}nH_2O$ shows a specific capacity of 351 mAh g^{-1} at 0.3 A g^{-1} and long cycle life of 1000 cycles in this hybrid electrolyte due to the dissolution suppression of vanadium species.

In summary, great progress has been made in the development of V_2O_5 polymorphs in MIBs with capacities of over 250 mAh g^{-1} and good cycling stability. However, MIBs face challenges such as sluggish Mg-ion diffusion in host materials and the incompatibility of electrolytes with high-voltage V_2O_5 cathode and Mg anode. Moreover, the most common Mg-ion electrolytes show high corrosion to the battery casing and current collectors. The breakthrough of a new methoxyethyl-amine chelants-based electrolyte [121] brings new light to the development of high-voltage Mg systems, which greatly enables the usage of both high-voltage $Mg_{0.15}MnO_2$ cathode and Mg metal anode with high reversibility and stable cycling. The application of V_2O_5 polymorphs in such a new electrolyte is not reported yet. More efforts should be done to improve the overall electrochemical performance (capacity, rate capability, and cycling stability) by the engineering of V_2O_5 polymorph hosts, electrolytes, and electrode/electrolyte interphase.

Calcium-ion batteries (CIBs)

In 2016, Palacín et al. [122] carried out pioneering work on the reversible Ca stripping/plating using 0.45 M $Ca(BF_4)_2$ in EC:PC at 100°C with high stability window >3.5 V and opened the door to new rechargeable battery technology. At RT, the study of V_2O_5 in

CIBs dates back to 2003, when Hayashi et al. [123] showed both crystalline and amorphous V_2O_5 delivering discharge capacity of more than 400 mAh g^{-1} in $Ca(ClO_4)_2$ in acetonitrile (only the first discharge curve is shown) for CIBs. However, this electrolyte only enables anodic Ca dissolution, but no cathodic deposition, when metallic Ca is used as a negative electrode. Ex situ XRD demonstrates the new phase formation during Ca^{2+} insertion and the recovery after Ca^{2+} deinsertion. Palacín et al. [104] studied Mg^{2+} and Ca^{2+} insertion into α-V_2O_5 under diverse conditions, where both dry/wet alkyl carbonate-based electrolytes are used for electrochemical characterization at RT and 100°C. They claimed that a proton-inserted V_2O_5 phase forms during cycling and the new orthorhombic phase formation of V_2O_5 at 100°C in alkyl carbonate is most likely attributed to degradation by water and temperature. However, δ-MgV_2O_5 and α-CaV_2O_5 prepared by solid-state reaction are electrochemically and chemically inactive. Sakurai et al. [124] investigated the effect of water in the electrolyte on Ca^{2+} (de) intercalation into α-V_2O_5. The results display that the overpotential gradually reduces with the increase of water and that H^+ cointercalation only contributes a small portion of capacity while its amount differs depending on the amount of water. Later on, the same group [125] studied different electrolytes using V_2O_5 cathode for CIBs. They claimed that the electrochemical performance strongly depends on the molar ratio of the contact ion pair (CIP) in the total ionic species. Despite the low coulombic efficiency, V_2O_5 shows the highest capacity in 0.5 M $Ca(TFSI)_2$/triglyme, which has relatively small molar ratios of CIP.

Na-doped $NH_4V_4O_{10}$ [126] with reduced particle size shows an initial capacity of 150 mAh g^{-1}, without notable fading after 100 cycles. Moreover, a full cell consisting of Na-doped $NH_4V_4O_{10}$ cathode and Mn-bdcNH_2 anode delivers a maximum discharging capacity of 75 mAh g^{-1} with no capacity fading after 100 cycles. $V_2O_5{\cdot}1.6H_2O$/PC composite [127] in 0.4 M $Ca(ClO_4)_2$/PC electrolyte offers a high capacity of 465 mAh g^{-1}, which is much higher than that obtained without PC, demonstrating the critical role of this solvent. Mai et al. [128] reported bilayered $Mg_{0.25}V_2O_5{\cdot}H_2O$ with a large interlayer spacing of 10.8 Å, which exhibits a reversible discharge capacity of ~120 mAh g^{-1} at 20 mA g^{-1} and good cycling stability (capacity retention of 87% after 500 cycles) (Figure 8). The good cycling stability is attributed to a small variation (~0.09 Å) of interlayer spacing during Ca^{2+} (de)intercalation.

In addition, few works also focus on aqueous CIBs using vanadium oxide materials such as bilayered $V_2O_5{\cdot}0.63H_2O$ [129], V_3O_8, CaV_2O_6, and $CaV_6O_{16}{\cdot}7H_2O$ [130]. Hong et al. [129] synthesized bilayered $V_2O_5{\cdot}0.63H_2O$ via electrodeposition on graphite foil for aqueous CIBs. The material shows a high reversible capacity of 204 mAh g^{-1} at 0.1 C rate in aqueous 1 M $Ca(NO_3)_2$ and capacity retention of 86% (at 5 C) after 350 cycles. The combination of bulk intercalation and surface pseudo-capacitance reactions is proposed for Ca^{2+} storage. $CaV_6O_{16}{\cdot}7H_2O$ [130] shows a high capacity of 205 mA h g^{-1} with long cycle life and high-rate performance upon Ca-ion (de)intercalation.

In summary, V_2O_5 polymorphs already show their promising aspects regarding multiple redox reactions, cycling stability, and abundant resources. However, many efforts are needed to further improve their capacity, rate capability, and diffusion kinetics by adopting the host materials. The development of noncorrosive electrolytes [121, 131] will surely push forward the combination of high-voltage V_2O_5 and Ca metal. Moreover, more efforts should also be made on the electrode/electrolyte interphases, and the development of suitable electrolytes and anode materials due to the reactive property of Ca metal via appropriate strategies.

Zinc-ion batteries

Zinc metal is abundant in the earth's crust with a high specific capacity (820 mA h g^{-1}) and high volumetric capacity (5854 mA h cm^{-3}), making it promising as an anode. It also has sufficiently high overpotentials with respect to the hydrogen evolution, overcompensating the negative value of −0.76 V versus SHE that makes it usable in water [132] and, therefore, a suitable anode for aqueous Zinc-ion battery system (AZIBs) [11a]. Compared with nonaqueous electrolytes, aqueous electrolytes provide higher ionic conductivity (up to 1 S cm^{-1}), lower activation energy for charge transfer [133] as well as high safety. Moreover, water-based electrolytes are nontoxic and reduce the manufacturing costs of AZIBs, making them very promising. However, the higher reduction potential of Zn^{2+} (−0.76 V vs. SHE) would result in a rather low output voltage in a full-cell configuration. Another drawback is that the water decomposition limits the electrochemical stability window (~1.23 V) of aqueous electrolytes [11b]. Moreover, although the radii of Zn^{2+} (0.74 Å) is similar to Li^+ (0.76 Å), the higher charge density of Zn^{2+} results in low solid-state mobility in the electrode bulk [134]. Overall, more efforts need to be made to develop high-performance electrodes and electrolytes for AZIBs.

The first application of V_2O_5 for Zn-ion batteries was reported by Zhu et al. [89b] in 1987, where Mg/V_2O_5 and Zn/V_2O_5 cells were built using Mg- and Zn-montmorillonite solid electrolytes. Later on, Smyrl et al. [113] demonstrated that V_2O_5 aerogel can not only uptake Mg^{2+} and Al^{3+} but also Zn^{2+} inside the host via chemical intercalation with 2.5 mol of Zn^{2+}, per mole V_2O_5 aerogel. V_2O_5 is a very popular cathode for AZIBs due to its layered structure and large theoretical capacity (589 mA h g^{-1}, based on 2 Zn^{2+} insertion) [133]. It also possesses multiple crystal structures, has a low cost, and has a suitable flat potential at 0.8–1.0 V versus Zn^{2+}/Zn. Among the available polymorphs of V_2O_5, α-type and hydrated V_2O_5 received the most attention. A reversible Zn/V_2O_5 full cell using a nonaqueous electrolyte was reported to deliver a capacity of 170 mA h g^{-1} at 0.85 V [135]. Meanwhile, Nazar et al. [132] opened the door to Zn/vanadium-based oxides for AZIBs, consisting of $Zn_{0.25}V_2O_5{\cdot}nH_2O$ cathode with a Zn^{2+}/water co(de)intercalation as shown in Figure 9a. They found that the structure of pristine $Zn_{0.25}V_2O_5{\cdot}nH_2O$ changes through water intercalation upon immersion in the electrolyte,

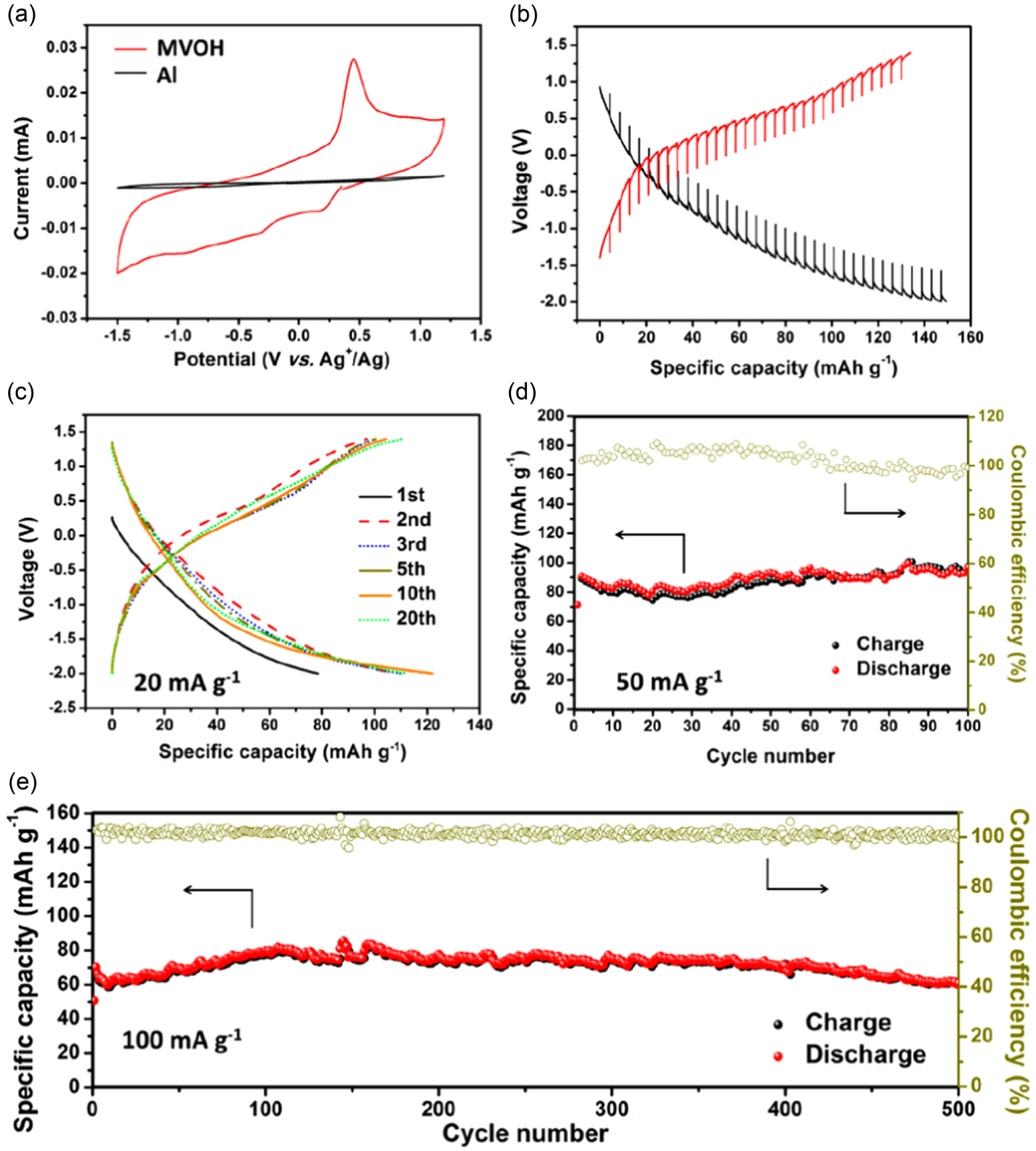

FIGURE 8 Electrochemcial properties of $Mg_{0.25}V_2O_5{\cdot}H_2O$ upon Ca^{2+} (de)intercalation: (a) CV curves based on the three-electrode cell with AC counter electrode and Ag^+/Ag reference electrode, (b) Galvanostatic intermittent titration technique measurement based on the two-electrode cell, (c) charge-discharge profiles of $Mg_{0.25}V_2O_5{\cdot}H_2O$//AC cell at 20 mA g^{-1}, and (d, e) cycling performance at 50 and 100 mA g^{-1}. Reproduced with permission [128]. Copyright 2019 American Chemical Society. AC, activated carbon.

resulting in an expanded interlayer spacing that facilitates the Zn^{2+} intercalation. Since then, many vanadium-based oxides cathode materials have been studied in AZIBs, including LiV_3O_8, $H_2V_3O_8$, tunnel-structured VO_2, spinel-structured ZnV_2O_4, $NH_4V_3O_8$, $Na_2V_6O_{16}{\cdot}3H_2O$, V_2O_5, and so on [136], where several reviews have reported the developments and challenges of cathode materials and electrolytes [11b, 133, 134, 136, 137]. Among them, V_2O_5 has received intense attention, and the developments and perspectives of V_2O_5 cathode in AZIBs were reviewed in 2020 by Luo et al. [137f], including its storage mechanism, composition optimization, application in flexible AZIBs, and their perspectives on future development trends. In the following, we briefly summarize the storage mechanism and recent advances.

Liang et al. [138] studied the behavior of α-V_2O_5/Zn cell in different types and concentrations of electrolytes. α-V_2O_5/Zn cell with 3 M $ZnSO_4$ electrolyte delivers a capacity of 224 mA h g^{-1} at 100 mA g^{-1} (this is only normalized by the cathode). They proposed a new phase formation of $Zn_xV_2O_5$ upon Zn insertion confirmed via ex situ XRD. Zhang et al. [139] showed an improved performance of V_2O_5 in 3 M $Zn(CF_3SO_3)_2$ electrolyte with a capacity of 470 mA h g^{-1}

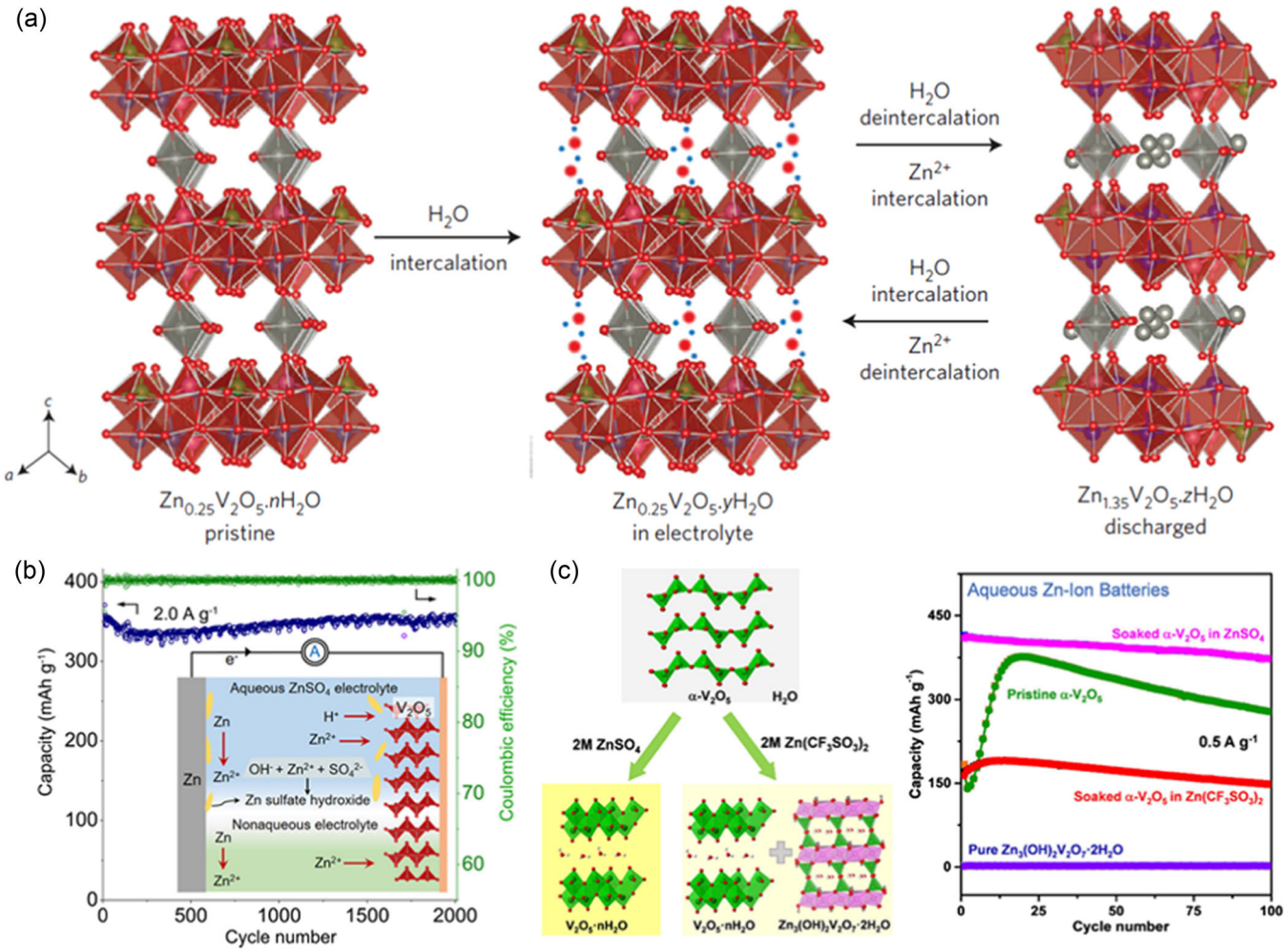

FIGURE 9 (a) Scheme of water intercalation into $Zn_{0.25}V_2O_5{\cdot}nH_2O$ immersed in electrolyte and reaction mechanism of $Zn_{0.25}V_2O_5{\cdot}nH_2O$ upon cycling. Reproduced with permission from Kundu et al. [132]. Copyright 2016 Springer Nature. (b) Schematic illustration and cycling performance of V_2O_5 in 3 M $ZnSO_4$ electrolyte at 2.0 A g^{-1}. Reproduced with permission from Dong et al. [141]. Copyright 2020 American Chemical Society. (c) Scheme of the dissolution and phase transformation mechanisms of α-V_2O_5 in aqueous $ZnSO_4$ and $Zn(CF_3SO_3)_2$ Electrolytes and cycling performance after different treatments. Reproduced with permission from Zhu et al. [146]. Copyright 2021 American Chemical Society.

at 0.2 A g^{-1} and proposed the coinsertion of hydrated Zn ions into the structure. Then Chen et al. [140] demonstrated the phase transition from V_2O_5 to zinc pyrovanadate for the first discharge and reversible Zn^{2+} (de)insertion of the formed zinc pyrovanadate during subsequent cycles. Reversible proton and Zn^{2+} cointercalation into V_2O_5 was also reported in aqueous $ZnSO_4$ electrolyte [141], involving the formation of $ZnSO_4Zn_3(OH)_6{\cdot}5H_2O$ (Figure 9b). Then, Li et al. [142] reported that yolk–shell microspheres V_2O_5 initially showed an interlayer spacing expansion to $V_2O_5{\cdot}nH_2O$ through water and H^+ insertion and demonstrated the formation of $Zn_xV_2O_5{\cdot}nH_2O$ during cycling. Moreover, zinc pyrovanadate was formed after being soaked in the electrolyte. Fu et al. [143] further clarified the structural evolution of orthorhombic V_2O_5 upon Zn^{2+} (de)insertion via in operando techniques and confirmed that two solid-solution reactions and one 2-phase reaction occur during the discharged process with the appearance of by-product ($ZnSO_4Zn_3(OH)_6{\cdot}5H_2O$ and $Zn_{3+\delta}(OH)_2V_2O_7{\cdot}2H_2O$). Chung et al. [144] directly visualized the co-intercalation of Zn^{2+} and H_2O into V_2O_5 in an aqueous $ZnSO_4$ electrolyte using atomic-column-resolved scanning transmission electron microscopy and demonstrated the formation of multiple intermediate phases (VO_2 and VO-rocksalt-type) and structurally topotactic correlation between the phases.

However, V_2O_5 suffers from poor ionic conductivity, a fragile layered structure, and dissolution in aqueous solutions [11b], leading to inferior cycling stability [145]. Huang et al. [146] investigated the dissolution mechanisms and phase transformation phenomenon of α-V_2O_5 (Figure 9c). They found the dissolution of V_2O_5 in $ZnSO_4$ led to phase transition to a hydrated $V_2O_5{\cdot}1.75H_2O$ xerogel, while in Zn $(CF_3SO_3)_2$, major hydrated $V_2O_5{\cdot}1.75H_2O$ xerogel and minor harmful $Zn_3(OH)_2V_2O_7{\cdot}2H_2O$ (ZVO) were formed, where H-V_2O_5 is the active material for Zn^{2+}/H^+ storage. Other researchers also confirmed the phase transition of V_2O_5 to ZVO, but they believed that

ZVO was still electrochemically active [147]. Although the role of ZVO above is controversial, these studies play an integral role in investigating the dissolution mechanism of V_2O_5.

Meanwhile, $V_2O_5{\cdot}nH_2O$ and cations pre-intercalated $V_2O_5{\cdot}nH_2O$ have gained a lot of attention due to the large interlayered spacing, where the crystal water can shield charge and preintercalated cations M^{n+} can help to maintain the structural stability during cycling. The preintercalated cation, M^{n+} includes alkali metal, alkaline earth metal ions and other metal ions (Li^+, Na^+, K^+, Mg^{2+}, Zn^{2+}, Ca^{2+}, Ba^{2+}) [148], transition metal ions (Fe^{2+}, Co^{2+}, Ni^{2+}, Mn^{2+}, Ag^+) [149], nonmental ion (NH_4^+) [150]. The specific capacity and the long-cycle performance of these kinds of materials are greatly improved compared to V_2O_5. For example, $Li_xV_2O_5{\cdot}nH_2O$ [148a] (232 mA h g^{-1} after 500 cycles at 5 A g^{-1}, and 192 mA h g^{-1} after 1000 cycles at 10 A g^{-1}), $Mg_{0.34}V_2O_5{\cdot}0.84H_2O$ [148b] (352 mA h g^{-1} at 100 m Ag^{-1}, and ~97% capacity retention for at least 2000 cycles at 5000 mA g^{-1}). In addition to cations/water pre-intercalation, morphology regulation [140, 142, 151], carbon materials or conductive polymer composite [152] and high-concentration electrolytes [145] have also been used to overcome the dissolution, structure instability, and poor ionic conductivity of V_2O_5, thus improving the zinc storage properties of V_2O_5.

In summary, AZIBs are one of the most promising systems in recent years due to their high safety, low cost, low toxicity, and simple fabrication. V_2O_5 polymorphs have demonstrated their promising aspects in the application of AZIBs because of their high capacity (>300 mA h g^{-1}) and long cycle life. However, V_2O_5 materials still suffer from low operating voltage (~1 V), vanadium dissolution, poor electrical conductivity, sluggish kinetics, and structural instability. Moreover, special attention should also be given to the surface passivation, zinc dendrites formation, and self-corrosion of zinc in electrolytes to speed up its commercial progress.

Al-ion batteries

The first attempt and success of intercalation of Al^{3+} into V_2O_5 dates back to 1998 when Le and coauthors [113] performed chemical intercalation of Al^{3+} into V_2O_5 aerogel to form an $Al_xV_2O_5$ compound. They assembled a cell consisting of two types of V_2O_5: a virgin one and a preintercalated one (Figure 10a) in $Al(CF_3SO_3)_3$ (triflate)/propylene carbonate electrolyte. Although the electrolyte was not optimized, they successfully demonstrated the exchange of 3.3 equivalents of Al^{3+} between the two vanadium oxide electrodes. To highlight the relevance of this discovery, it is important to mention that in 1998 rechargeable aluminum batteries with reversible Al stripping/plating electrolytes were not existing yet.

The scientific community had to wait until 2011 to see the first "rechargeable aluminum battery" based on an aluminum negative electrode and V_2O_5 nanowires [153] (Figure 10b). The probable delay was due to the difficulty in the design of an appropriate electrolyte, which could enable a reversible plating and stripping of aluminum at the metal negative electrode. Today, the most promising electrolyte is based on a mixture of EMimCl ionic liquid and $AlCl_3$ salt in proportion 1:1.5 [154].

This ratio is extremely important because it enables the formation of the proper amount of $Al_2Cl_7^-$ complex, which is the specie responsible for Al plating and stripping. However, with the knowledge available in 2011, the first aluminum battery was based on an electrolyte composed of $EMImCl/AlCl_3$ with a ratio of 1:1.1 (less acidic). The current collector was based on stainless steel. The combination of these two factors could have led to a limited number of cycles (only 20 cycles are shown in this publication) [153].

Two years later, Reed and Menke demonstrated that the obtained capacity was instead due to the corrosion of the stainless steel current collector [155]. From that moment, a critical discussion questioning the electrochemical activity of V_2O_5 in ionic liquid electrolytes was started [156].

Table 1 summarizes the available experimental data in chronological order from top to down. An important factor when evaluating V_2O_5 together with an aluminum anode is the choice of the electrolyte (which should enable Al plating and stripping). The electrolyte (the highly corrosive $AlCl_3$/EMimCl mixture) is then connected to the stability and the choice of all other components like the binder, current collector, and additives, which, in turn, influences the side reactions and the correct evaluation of the V_2O_5 behavior. For a correct evaluation, the redox activity of the aluminum negative electrode in the corresponding electrolyte should also be

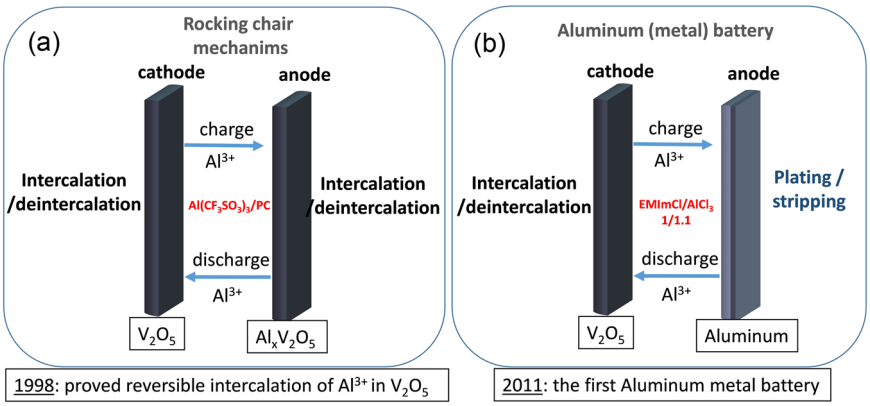

FIGURE 10 Schematic representation of the (a) $V_2O_5/Al_xV_2O_5$ "rocking chair" battery and (b) the aluminum/V_2O_5 battery.

TABLE 1 Experimental reports on the electrochemical activity of V_2O_5 toward Al^{3+} intercalation

Cathode	Current collector	Anode	Electrolyte	Cycles number	Capacity/ m Ah g^{-1}	Remarks	References	Publication year
V_2O_5 Xerogel	Carbon foil	$Al_xV_2O_5$	0.1 M $Al(CF_3SO_3)_3$/PC	-	-	Redox activity from CV	[113]	1998
V_2O_5 nanowires	Stainless Steel	Al	$Al(CF_3SO_3)_3$/PC/THF	0	0	No capacity: the electrolyte does not allow Al plating/stripping	[153]	2011
V_2O_5 nanowires	Stainless Steel	Al	EMImCl/$AlCl_3$ (1:1.1)	20	280		[153]	2011
V_2O_5 aerogel	Stainless Steel	Al	EMImCl/$AlCl_3$ (1:1.2)	-	-	Redox activity from CV	[155]	2013
V_2O_5 aerogel	Pt	Al	EMImCl/$AlCl_3$ (1:1.2)	-	-	No redox peaks in the CV	[155]	2013
V_2O_5 nanowires—binder free	Ni foam	Al	[BMIM]Cl/$AlCl_3$ (1:1.1)	5	200		[156a]	2015
V_2O_5 nanowires—PTFE	Ni foam	Al	[BMIM]Cl/$AlCl_3$ (1:1.1)	5	85		[156a]	2015
V_2O_5 nanowires—PVDF	Ni foam	Al	[BMIM]Cl/$AlCl_3$ (1:1.1)	5	40	Demonstrated impact of PVDF degradation	[156a]	2015
Amorphous V_2O_5—carbon composite	Mo	Al	$AlCl_3$/dipropylsulfone/toluene (1:10:5 in mole ratio)	30	150		[156d]	2015
V_2O_5 Xerogel	Carbon paper	Glassy Carbon	1 M $AlCl_3/H_2O$	12	140		[158]	2016
V_2O_5 nanowires	Ni foam	Al	[BMIM]Cl/$AlCl_3$ (1:1.1)	10	50		[156b]	2017
V_2O_5 scaffolds	Mo	Al	EMImCl/$AlCl_3$ (1:1.5)	50	100/60 (at 0.5/2 A g^{-1})		[156c]	2020
V_2O_5 nanofibers/carbon composite	Mo	Al	EMImCl/$AlCl_3$ (1:1.3)	10	80	(mixed intercalation Al^{3+} on V_2O_5 and $AlCl_4^-$ in carbon	[156e]	2020

Abbreviations: PVDF, polyvinylidene difluoride; PTFE, polytetrafluoroethylene.

confirmed, which has been rarely reported in the papers dealing with cathode materials. It is nowadays accepted that Al is active when the molar ratio between $AlCl_3$ and the ionic liquid is >1.3 (which is the case only for references [156c] and [156e] of Table 1).

By summing up, the factors that need to be taken into account for the electrochemical activity of V_2O_5 are its intrinsic properties, such as: (1) higher interlayer spacing facilitates the insertion of the trivalent ion [113, 157], (2) amorphous V_2O_5 seems to favor the reaction with Al^{3+} compared with crystallinity one [156d, 158], (3) small pores lengths translate in short diffusion distance. [113]

Further research should be done considering the combination of the appropriate cell, electrode, and electrolyte components to correctly assess the capacity and cycling stability of V_2O_5 and to make it a plausible cathode material candidate for next-generation aluminum batteries.

Nonmetallic cations batteries (proton and ammonium)

Besides the above metallic cations charge carriers, batteries based on nonmetal cations, for example, proton (H^+/H_3O^+) and ammonium (NH_4^+) ions have received much attention due to the abundant resources and sustainability of the contained elements.

Ji et al. [13b] summarized the most advances of proton ion batteries, including cathode, anode, and electrolytes, and proposed their viewpoints on its current challenges and future directions. The application of protons as charge carriers dates back to the lead-acid batteries in 1859, involving the reaction $Pb + PbO_2 + 4H^+ + 2SO_4^{2-} \leftrightarrow 2PbSO_4 + 2H_2O$ [159]. Proton insertion also involved the Ni-Cd (1899) and Ni-MH batteries (1967), where protons are released from neutral water dissociation [160]. Recently, proton coinsertion has been discovered and discussed in both nonaqueous (Li^+, Mg^{2+}, Ca^{2+}) [103, 104, 124, 161] and aqueous (Li^+, Zn^{2+}) [141, 146, 162] batteries. Currently, PBAs [163], metal oxides [141, 146, 162b, 162c, 164], and organic compounds [13b] have been intensively studied as proton-storage cathode materials. Although proton batteries usually do not provide as high energy density as that of the nonaqueous batteries, they often show superhigh rate capability up to 4000 C and super long cycle of 0.73 million [163a]. Moreover, proton batteries can exhibit outstanding low-temperature performance at −78°C and even −88°C despite their low capacity.

Pioneering work on NH_4^+ ions batteries was first reported by Cui et al. [165] in 2012, where they studied the various guest intercalation (Li^+, Na^+, K^+, and NH_4^+) in PBAs host materials. Since then, many efforts have been made concerning electrode materials, including vanadium-based oxides, manganese-based compounds, and PBAs [13a, 13c, 166]. Passerini et al. [13c] reviewed the most advances in ammonium (NH_4^+) ions batteries, including cathode, anode, and electrolytes, and also proposed possible solutions to overcome its current limitations. Ji et al. [167] investigated bilayered V_2O_5 ($V_2O_5{\cdot}nH_2O$) cathode for NH_4^+ storage and showed the H bonding between NH_4^+ and bilayered V_2O_5 with pseudocapacitive behavior, whose storage is much stronger and faster than that of K^+. Moreover, $V_2O_5{\cdot}nH_2O$ still delivers 58 mAh g^{-1} with capacity retention of 80% after 30,000 cycles at 50 C. Wang et al. [168] designed a flexible aqueous ammonium-ion full cell consisting of $NH_4V_4O_{10}$/carbon fiber and polyaniline/carbon fiber with high rate capability and long cycle life. The full cell shows a high initial capacity up to 167 mA h g^{-1} at 0.1 A g^{-1} and maintains a capacity of 66 mA h g^{-1} after 1000 cycles. Mai et al. [169] prepared polyaniline-intercalated vanadium oxide, displaying the highest reported capacity of 307 mA h g^{-1} at 0.5 A g^{-1}. The reversible insertion/deinsertion of NH_4^+ corresponded to H bond formation/breaking with V = O groups as demonstrated by in situ FT-IR and XPS.

As a result, proton and ammonium ion batteries hold their advantages, such as abundant resources and inherently safe, which show good capability and long cycling stability. However, it remains big challenge regarding energy density compared with other batteries using metallic anode. In addition, most cathode materials do not contain proton/NH_4^+ ions in their original structure and aqueous electrolytes suffer from intrinsic restriction of the low ESW. Therefore, the optimization of suitable cathode/anode and electrolytes with extended ESW should be carried out to improve the overall energy density of the full cells.

APPROACHES TO IMPROVE THE PERFORMANCE OF V_2O_5

V_2O_5-based materials have shown their great electrochemical performance and potential for practical application for various type of batteries and Table 2 provides some examples to show the type of M-battery and reports the key performance (e.g., electrolyte, counter electrode, capacity, cycle number, current used, and average voltage). Despite its advantages, V_2O_5 suffers from serious issues such as low electronic conductivity (10^{-2}–10^{-3} S cm^{-1}) [170], intrinsic low diffusion coefficient (10^{-12}–10^{-13} cm^2 s^{-1}) [28c, 170] and dissolution, which results in poor cycling stability of this material and retarders its practical application. Moreover, V_2O_5 is subjected to a low average voltage compared with other cathode materials, such as MnO_2. Numerous efforts have been made to overcome these problems, including the synthesis of nanostructured materials, heterogeneous structures (including surface coating, composites), and cation doping (Figure 11). Moreover, special attention should be paid to other factors such as the selection/engineering of the appropriate cell, the counter electrode, and electrolyte components to obtain reliable results for further research.

(1) Nanostructured V_2O_5. Numerous nanostructured V_2O_5 materials (0D, 1D, 2D, 3D) were synthesized to improve the electrochemical performance, including cycling stability and rate capability, since nano-sized materials offer short diffusion lengths for cation insertion and facilitate the transport kinetics of electrons, resulting in higher capacities [172]. The small particle size and the large specific area increase the contact area between the electrode and electrolyte, which is beneficial for rate capability [172a, 173].

TABLE 2 V_2O_5-based materials in typical M-ion systems and their remarkable electrochemical performance parameters

Cathode	Batteries	Electrolyte@ Counter electrode	Specific capacity/current	Capacity retention/cycle number/current	Average voltage	References
$V_2O_5{\cdot}nH_2O$	NIBs	1 M $NaClO_4$ in PC @ Na	250 mAh g^{-1}/20 mA g^{-1}	85%/320/20 mA g^{-1}	3 V	[43a]
V_2O_5 nanorod @rGO	KIBs	1 M KPF_6 in EC:DEC @ Na	222 mA g^{-1}/147 mA g^{-1}	80%/500/147 mA g^{-1}	~2.7 V	[68]
$NaV_8O_{20}{\cdot}nH_2O$	Aqueous MIBs	1 M $Mg(ClO)_2$ in TEGDME/H_2O @ Pt	351 mAh g^{-1}/0.3 A g^{-1}	50%/1000/1.5 A g^{-1}	~2.7 V	[120]
$CaV_6O_{16}{\cdot}7H_2O$	Aqueous CIBs	4.5 M $Ca(NO_3)_2$ (pH adjusted to 10 with $Ca(OH)_2$) @activated carbon	205 mAh g^{-1}/12.5 mA g^{-1}	97%/200/150 mA g^{-1}	~2.8 V	[130]
V_2O_5/GO	Aqueous ZIBs	3 M $Zn(CF_3SO_3)_2$ @Zn	525 mAh g^{-1}/0.1 A g^{-1}	90.8%/10,000/20 A g^{-1}	~0.8 V	[171]
V_2O_5-Ni foam	AIBs	[BMIM]Cl/$AlCl_3$(1:1.1) @ Al	239 mAh g^{-1}/44.2 mA g^{-1}	77%/5/44.2 mAg^{-1}	~0.6 V	[156a]
Prussian blue analogue	proton batteries	2.0 M H_2SO_4 @activated carbon	95 mAh g^{-1}/95 mAg^{-1}	60%/0.73 million/47.5 A g^{-1}	~0.7 V	[163a]
Polyaniline-intercalated V_2O_5	ammonium ion batteries	0.5 M $(NH_4)_2SO_4$@ Pt	307 mA h g^{-1} at 0.5 A g^{-1}	42%/100/5 A g^{-1}	~0.2 V versus SCE	[169]

Abbreviations: CIB, calcium-ion battery; KIB, potassium-ion battery; MIB, magnesium-ion battery; NIB, Na-ion battery; ZIB, zinc-ion battery; AIB, aluminum-ion battery; SCE, saturated calomel electrode.

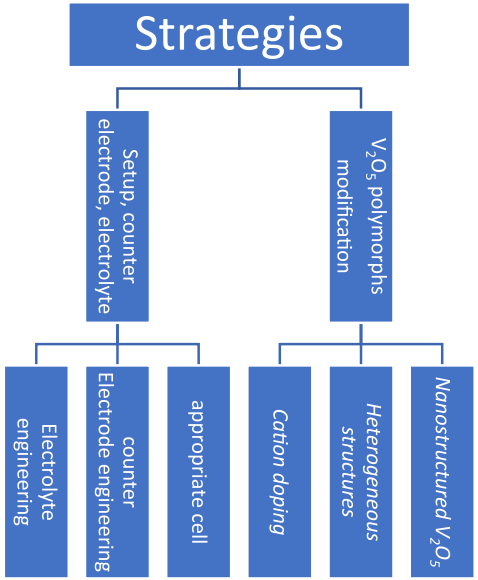

FIGURE 11 Schematic diagram of various engineering strategies to improve the electrochemical performance of V_2O_5 polymorphs.

(2) Heterogeneous structures. Heterogeneous structured materials, consisting of multinanocomponents, surface-coated materials, and composites, are currently regarded as very promising materials for the development of electrochemical EESs, due to their synergic properties, which arise from the integration of multi-nanocomponents, each tailored to satisfy a different requirement, such as high conductivity and high energy density, as well as outstanding mechanical stability [174].

(3) Cation doping. The structure and electronic state of electrode materials can be greatly influenced by the doping, including (1) increased electronic conductivity due to the formation of a lower oxidation state of V (V^{3+} and V^{4+}); (2) the formation of $[MO_6]$ octahedral units that can stabilize the layer structure of V_2O_5 during cycling; (3) facilitating charge transfer and the ion diffusion of V_2O_5 by expanding the interlayer spacing; (4) reducing the particles size and alter the morphology, improving the electrochemical performance of V_2O_5 [15b,175]. However, the excess dopant may block the pathway for the inserted ions and induce impurity or a second phase, thus reducing the capacity of the materials. Note that cation doping can also enhance the average voltage of V_2O_5 as compared with vanadate cathodes [137h].

Furthermore, other strategies such as the selection of the appropriate cell, counter electrode engineering, and electrolyte engineering should be considered to improve the electrochemical performance of V_2O_5 polymorphs. Especially, the appropriate cell/setup is critical to evaluate the performance of V_2O_5 due to the corrosion of the current collector/cell casing in electrolytes in some specific electrolytes (i.e., electrolytes for Mg and Al batteries). Surface and interface engineering of the counter electrode is vital to enable reversible metal stripping/plating, to suppress dendrites growth, and to reduce the side reaction between the metal and electrolyte, thus improving the overall performance of V_2O_5 polymorphs. The electrolyte plays an important role in controlling the performance of cells because of the direct contact with both the cathode and anode materials. It remains a great challenge to regulate a cathode/

anode compatible electrolyte to overcome the challenges of both the cathode and anode [176], such as electrolyte decomposition, cathode dissolutions, dendrites growth, and side reactions.

SUMMARY AND OUTLOOK

Vanadium pentoxide (V_2O_5) attracted much attention as host materials for post-Li batteries because of their rich structure, high capacity, easy preparation, and adequate safety, including α-, β-, δ-, γ-, ζ-, and ε-V_2O_5 as well as hydrate V_2O_5 ($V_2O_5{\cdot}nH_2O$). Among these polymorphs, α-V_2O_5 and bilayered V_2O_5 have received the most attention in various guest insertions. However, V_2O_5 exhibit poor electrochemical performance with limited capacity and cycling stability because of the intrinsic low conductivity of V_2O_5, structure degradation, and electrode dissolution. Numerous efforts have been made to overcome these issues, including the synthesis of nanostructured materials, heterogeneous structures (including surface coating, composites), and cation doping. Further research should be done by considering the combination of the appropriate cell, electrolyte, and electrode components to improve the capacity and cycling stability of V_2O_5 and to make it possible for commercialization in next-generation batteries.

ACKNOWLEDGMENTS

This work contributes to the research performed at CELEST (Center for Electrochemical Energy Storage Ulm-Karlsruhe) and was partially funded by the Deutsche Forschungsgemeinschaft (DFG, German Research Foundation) under Germany´s Excellence Strategy—EXC 2154—Project ID 390874152 (POLiS Cluster of Excellence). H.Z. acknowledges the financial support from the China Scholarship Council (No. 202006170127) during the visiting PhD study in KIT. Open Access funding enabled and organized by Projekt DEAL.

CONFLICT OF INTEREST

The authors declare no conflict of interest.

DATA AVAILABILITY STATEMENT

The data that support the findings of this study are available from the corresponding author upon reasonable request.

ORCID

Qiang Fu http://orcid.org/0000-0002-2507-5477

REFERENCES

[1] a) J. Muldoon, C. B. Bucur, T. Gregory, *Chem. Rev.* **2014**, *114*, 11683; b) D. Larcher, J. M. Tarascon, *Nat. Chem.* **2015**, *7*, 19; c) G. Jeong, Y.-U. Kim, H. Kim, Y.-J. Kim, H.-J. Sohn, *Energy Environ. Sci.* **2011**, *4*, 1986; d) B. Scrosati, J. Hassoun, Y.-K. Sun, *Energy Environ. Sci.* **2011**, *4*, 3287; e) Z. Yang, J. Zhang, M. C. W. Kintner-Meyer, X. Lu, D. Choi, J. P. Lemmon, J. Liu, *Chem. Rev.* **2011**, *111*, 3577.

[2] a) C. Liu, F. Li, L.-P. Ma, H.-M. Cheng, *Adv. Mater.* **2010**, *22*, E28; b) B. Dunn, H. Kamath, J.-M. Tarascon, *Science* **2011**, *334*, 928.

[3] a) J. Liu, *Adv. Funct. Mater.* **2013**, *23*, 924; b) H. Pan, Y.-S. Hu, L. Chen, *Energy Environ. Sci.* **2013**, *6*, 2338; c) W. Tang, Y. Zhu, Y. Hou, L. Liu, Y. Wu, K. P. Loh, H. Zhang, K. Zhu, *Energy Environ. Sci.* **2013**, *6*, 2093.

[4] a) Y. Wang, J. Yi, Y. Xia, *Adv. Energy Mater.* **2012**, *2*, 830; b) J. B. Goodenough, K.-S. Park, *J. Am. Chem. Soc.* **2013**, *135*, 1167; c) J.-Y. Hwang, S.-T. Myung, Y.-K. Sun, *Chem. Soc. Rev.* **2017**, *46*, 3529; d) K. Kubota, M. Dahbi, T. Hosaka, S. Kumakura, S. Komaba, *Chem. Rec.* **2018**, *18*, 459; e) M. S. Whittingham, *Chem. Rev.* **2004**, *104*, 4271.

[5] H. Kim, J. Hong, K.-Y. Park, H. Kim, S.-W. Kim, K. Kang, *Chem. Rev.* **2014**, *114*, 11788.

[6] N. Yabuuchi, K. Kubota, M. Dahbi, S. Komaba, *Chem. Rev.* **2014**, *114*, 11636. https://doi.org/10.1021/cr500192f

[7] J. Deng, W.-B. Luo, S.-L. Chou, H.-K. Liu, S.-X. Dou, *Adv. Energy Mater.* **2018**, *8*, 1701428.

[8] T. Hosaka, K. Kubota, A. S. Hameed, S. Komaba, *Chem. Rev.* **2020**, *120*, 6358.

[9] P. Saha, M. K. Datta, O. I. Velikokhatnyi, A. Manivannan, D. Alman, P. N. Kumta, *Prog. Mater. Sci.* **2014**, *66*, 1.

[10] a) M. E. Arroyo-de Dompablo, A. Ponrouch, P. Johansson, M. R. Palacín, *Chem. Rev.* **2020**, *120*, 6331; b) B. Ji, H. He, W. Yao, Y. Tang, *Adv. Mater.* **2021**, *33*, 2005501.

[11] a) B. Tang, L. Shan, S. Liang, J. Zhou, *Energy Environ. Sci.* **2019**, *12*, 3288; b) X. Jia, C. Liu, Z. G. Neale, J. Yang, G. Cao, *Chem. Rev.* **2020**, *120*, 7795.

[12] a) G. A. Elia, K. Marquardt, K. Hoeppner, S. Fantini, R. Lin, E. Knipping, W. Peters, J.-F. Drillet, S. Passerini, R. Hahn, *Adv. Mater.* **2016**, *28*, 7564; b) J. Tu, W.-L. Song, H. Lei, Z. Yu, L.-L. Chen, M. Wang, S. Jiao, *Chem. Rev.* **2021**, *121*, 4903.

[13] a) G. Liang, F. Mo, X. Ji, C. Zhi, *Nat. Rev. Mater.* **2021**, *6*, 109; b) Y. Xu, X. Wu, X. Ji, *Small Structures* **2021**, *2*, 2000113; c) J. Han, A. Varzi, S. Passerini, *Angew. Chem. Int. Ed.* **2022**, *61*, e202115046.

[14] M. S. Whittingham, *J. Electrochem. Soc.* **1976**, *123*, 315.

[15] a) Y. Wang, K. Takahashi, K. H. Lee, G. Z. Cao, *Adv. Funct. Mater.* **2006**, *16*, 1133; b) J. Yao, Y. Li, R. C. Massé, E. Uchaker, G. Cao, *Energy Storage Mater.* **2018**, *11*, 205; c) C. Wu, Y. Xie, *Energy Environ. Sci.* **2010**, *3*, 1191.

[16] M. Sutradhar, J. A. L. Da Silva, A. J. L. Pombeiro, *Vanadium Catalysis*, The Royal Society of Chemistry, United Kingdom, **2021**, pp. 1. https://doi.org/10.1039/9781839160882-00001

[17] P. E. Tang, J. S. Sakamoto, E. Baudrin, B. Dunn, *J. Non-Cryst. Solids* **2004**, *350*, 67.

[18] R. Enjalbert, J. Galy, *Acta Crystallogr. C* **1986**, *42*, 1467.

[19] V. Shklover, T. Haibach, F. Ried, R. Nesper, P. Novák, *J. Solid State Chem.* **1996**, *123*, 317.

[20] Q. Fu, A. Sarapulova, L. Zhu, G. Melinte, A. Missyul, E. Welter, X. Luo, M. Knapp, H. Ehrenberg, S. Dsoke, *J. Energy Chem.* **2021**, *62*, 627.

[21] a) V. P. Filonenko, M. Sundberg, P.-E. Werner, I. P. Zibrov, *Acta Crystallogr. B* **2004**, *60*, 375; b) M. E. Arroyo y de Dompablo, J. M. Gallardo-Amores, U. Amador, E. Morán, *Electrochem. Commun.* **2007**, *9*, 1305; c) J. M. Gallardo-Amores, N. Biskup, U. Amador, K. Persson, G. Ceder, E. Morán, M. E. Arroyo y de Dompablo, *Chem. Mater.* **2007**, *19*, 5262.

[22] P. Balog, D. Orosel, Z. Cancarevic, C. Schön, M. Jansen, *J. Alloys Compd.* **2007**, *429*, 87.

[23] I. P. Zibrov, V. P. Filonenko, S. G. Lyapin, V. A. Sidorov, *High Press. Res.* **2013**, *33*, 399.

[24] J. M. Cocciantelli, P. Gravereau, J. P. Doumerc, M. Pouchard, P. Hagenmuller, *J. Solid State Chem.* **1991**, *93*, 497.

[25] a) P. M. Marley, T. A. Abtew, K. E. Farley, G. A. Horrocks, R. V. Dennis, P. Zhang, S. Banerjee, *Chem. Sci.* **2015**, *6*, 1712; b) J. V. Handy, Y. T. Luo, J. L. Andrews, N. Bhuvanesh, S. Banerjee, *Angew. Chem. Int. Ed.* **2020**, *59*, 16385.

[26] Y. Luo, S. Rezaei, D. A. Santos, Y. Zhang, J. V. Handy, L. Carrillo, B. J. Schultz, L. Gobbato, M. Pupucevski, K. Wiaderek, H. Charalambous, A. Yakovenko, M. Pharr, B.-X. Xu, S. Banerjee, *Proc. Natl. Acad. Sci. USA* **2022**, *119*, e2115072119.

[27] a) T. M. Tolhurst, B. Leedahl, J. L. Andrews, S. Banerjee, A. Moewes, *J. Mater. Chem. A* **2017**, *5*, 23694; b) A. Parija, Y. Liang, J. L. Andrews, L. R. De Jesus, D. Prendergast, S. Banerjee, *Chem. Mater.* **2016**, *28*, 5611.

[28] a) S. Kittaka, N. Uchida, H. Miyahara, Y. Yokota, *Mater. Res. Bull.* **1991**, *26*, 391; b) K. West, B. Zachau-Christiansen, T. Jacobsen, S. Skaarup, *Electrochim. Acta* **1993**, *38*, 1215; c) J. Livage, *Chem. Mater.* **1991**, *3*, 578; d) V. Petkov, P. N. Trikalitis, E. S. Bozin, S. J. L. Billinge, T. Vogt, M. G. Kanatzidis, *J. Am. Chem. Soc.* **2002**, *124*, 10157.

[29] a) N. Yabuuchi, K. Kubota, M. Dahbi, S. Komaba, *Chem. Rev.* **2014**, *114*, 11636; b) X. D. Xiang, K. Zhang, J. Chen, *Adv. Mater.* **2015**, *27*, 5343.

[30] a) J.-P. Parant, R. Olazcuaga, M. Devalette, C. Fouassier, P. Hagenmuller, *J. Solid State Chem.* **1971**, *3*, 1; b) M. S. Whittingham, *Prog. Solid State Chem.* **1978**, *12*, 41; c) A. S. Nagelberg, W. L. Worrell, *J. Solid State Chem.* **1979**, *29*, 345; d) J.-J. Braconnier, C. Delmas, C. Fouassier, P. Hagenmuller, *Mater. Res. Bull.* **1980**, *15*, 1797; e) C. Delmas, C. Fouassier, P. Hagenmuller, *Physica B+C* **1980**, *99*, 81; f) K. Mizushima, P. C. Jones, P. J. Wiseman, J. B. Goodenough, *Mater. Res. Bull.* **1980**, *15*, 783.

[31] K. West, *Solid State Ion.* **1988**, *28-30*, 1128.

[32] J. P. Pereira-Ramos, R. Messina, J. Perichon, *J. Electrochem. Soc.* **1988**, *135*, 3050.

[33] D. Muller-Bouvet, R. Baddour-Hadjean, M. Tanabe, L. T. N. Huynh, M. L. P. Le, J. P. Pereira-Ramos, *Electrochim. Acta* **2015**, *176*, 586.

[34] G. Ali, J. H. Lee, S. H. Oh, B. W. Cho, K.-W. Nam, K. Y. Chung, *ACS Appl. Mater. Interfaces* **2016**, *8*, 6032.

[35] E. Uchaker, Y. Z. Zheng, S. Li, S. L. Candelaria, S. Hu, G. Z. Cao, *J. Mater. Chem. A* **2014**, *2*, 18208.

[36] S. Liu, Z. Tong, J. Zhao, X. Liu, J. Wang, X. Ma, C. Chi, Y. Yang, X. Liu, Y. Li, *Phys. Chem. Chem. Phys.* **2016**, *18*, 25645.

[37] V. Raju, J. Rains, C. Gates, W. Luo, X. Wang, W. F. Stickle, G. D. Stucky, X. Ji, *Nano Lett.* **2014**, *14*, 4119.

[38] D. W. Su, S. X. Dou, G. X. Wang, *J. Mater. Chem. A* **2014**, *2*, 11185.

[39] Z. Zhao, D. Li, C. Wang, D. Fang, B. Wang, J. Li, H. Jin, *J. Alloys Compd.* **2022**, *895*, 162617.

[40] Y. Li, C. Liu, Z. Xie, J. Yao, G. Cao, *J. Mater. Chem. A* **2017**, *5*, 16590.

[41] F. Liu, X. Sun, Y. Liu, X. Song, J. Gao, G. Qin, *Appl. Surf. Sci.* **2019**, *473*, 873.

[42] a) S. Fleischmann, D. Leistenschneider, V. Lemkova, B. Krüner, M. Zeiger, L. Borchardt, V. Presser, *Chem. Mater.* **2017**, *29*, 8653; b) S. Tian, T. Cai, D. Wang, D. Kong, H. Ren, W. Xing, *IOP Conf. Ser.: Earth Environ. Sci.* **2021**, *692*, 022042.

[43] a) S. Tepavcevic, H. Xiong, V. R. Stamenkovic, X. B. Zuo, M. Balasubramanian, V. B. Prakapenka, C. S. Johnson, T. Rajh, *ACS Nano* **2012**, *6*, 530; b) D. Su, G. Wang, *ACS Nano* **2013**, *7*, 11218; c) H.-Y. Li, C.-H. Yang, C.-M. Tseng, S.-W. Lee, C.-C. Yang, T.-Y. Wu, J.-K. Chang, *J. Power Sources* **2015**, *285*, 418; d) A. Moretti, F. Maroni, I. Osada, F. Nobili, S. Passerini, *ChemElectroChem* **2015**, *2*, 529; e) A. Moretti, M. Secchiaroli, D. Buchholz, G. Giuli, R. Marassi, S. Passerini, *J. Electrochem. Soc.* **2015**, *162*, A2723; f) D. W. Su, S. X. Dou, G. X. Wang, *ChemSusChem* **2015**, *8*, 2877; g) H. Wang, X. Gao, J. Feng, S. Xiong, *Electrochim. Acta* **2015**, *182*, 769; h) Q. Wei, J. Liu, W. Feng, J. Sheng, X. Tian, L. He, Q. An, L. Mai, *J. Mater. Chem. A* **2015**, *3*, 8070; i) K. Zhu, C. Zhang, S. Guo, H. Yu, K. Liao, G. Chen, Y. Wei, H. Zhou, *ChemElectroChem* **2015**, *2*, 1660; j) H. L. Wang, X. X. Bi, Y. Bai, C. Wu, S. C. Gu, S. Chen, F. Wu, K. Amine, J. Lu, *Adv. Energy Mater.* **2017**, *7*, 1602720.

[44] K. Zhang, G. Gao, W. Sun, X. Liang, Y. Liu, G. Wu, *RSC Adv.* **2018**, *8*, 22053.

[45] R. Baddour-Hadjean, L. Thanh Nguyen Huynh, D. Batyrbekuly, S. Bach, J. P. Pereira-Ramos, *ChemSusChem* **2019**, *12*, 5192.

[46] M. Clites, J. L. Hart, M. L. Taheri, E. Pomerantseva, *ACS Appl. Energy Mater.* **2020**, *3*, 1063.

[47] R. Parmar, D. B. de Freitas Neto, E. Y. Matsubara, R. Gunnella, J. M. Rosolen, *Sustain. Energy Fuels* **2020**, *4*, 3951.

[48] a) A. Sarkar, S. Sarkar, T. Sarkar, P. Kumar, M. D. Bharadwaj, S. Mitra, *ACS Appl. Mater. Interfaces* **2015**, *7*, 17044; b) A. Sarkar, S. Sarkar, S. Mitra, *J. Mater. Chem. A* **2017**, *5*, 24929.

[49] X. Liu, B. Qin, H. Zhang, A. Moretti, S. Passerini, *ACS Appl. Energy Mater.* **2019**, *2*, 2786.

[50] M. Clites, B. W. Byles, E. Pomerantseva, *J. Mater. Chem. A* **2016**, *4*, 7754.

[51] R. Córdoba, A. Kuhn, J. C. Pérez-Flores, E. Morán, J. M. Gallardo-Amores, F. García-Alvarado, *J. Power Sources* **2019**, *422*, 42.

[52] R. Córdoba, J. Goclon, A. Kuhn, F. García-Alvarado, *Inorg. Chem.* **2020**, *59*, 16361.

[53] M. Safrany Renard, N. Emery, R. Baddour-Hadjean, J.-P. Pereira-Ramos, *Electrochim. Acta* **2017**, *252*, 4.

[54] M. Safrany Renard, R. Baddour-Hadjean, J. P. Pereira-Ramos, *Electrochim. Acta* **2019**, *322*, 134670.

[55] R. Baddour-Hadjean, M. Safrany Renard, J.-P. Pereira-Ramos, *J. Power Sources* **2021**, *482*, 229017.

[56] M. Safrany Renard, N. Emery, E. M. Roginskii, R. Baddour-Hadjean, J.-P. Pereira-Ramos, *J. Solid State Chem.* **2017**, *254*, 62.

[57] N. Emery, R. Baddour-Hadjean, D. Batyrbekuly, B. Laïk, Z. Bakenov, J.-P. Pereira-Ramos, *Chem. Mater.* **2018**, *30*, 5305.

[58] C. Liu, Z. G. Neale, G. Cao, *Mater. Today* **2016**, *19*, 109.

[59] R. Baddour-Hadjean, M. Safrany Renard, N. Emery, L. T. N. Huynh, M. L. P. Le, J. P. Pereira-Ramos, *Electrochim. Acta* **2018**, *270*, 129.

[60] N.uR. Lashari, M. Zhao, J. Wang, X. He, I. Ahmed, M. Liang, S. Tangsee, X. Song, *Energy Fuels* **2021**, *35*, 20394.

[61] Q. T. Qu, L. L. Liu, Y. P. Wu, R. Holze, *Electrochim. Acta* **2013**, *96*, 8.

[62] CATL Unveils Its Latest Breakthrough Technology by Releasing Its First Generation of Sodium-ion Batteries. https://www.catl.com/en/news/665.html

[63] K. Pfeifer, S. Arnold, J. Becherer, C. Das, J. Maibach, H. Ehrenberg, S. Dsoke, *ChemSusChem* **2019**, *12*, 3312.

[64] A. Eftekhari, *J. Power Sources* **2004**, *126*, 221.

[65] V. Mathew, S. Kim, J. Kang, J. Gim, J. Song, J. P. Baboo, W. Park, D. Ahn, J. Han, L. Gu, Y. Wang, Y.-S. Hu, Y.-K. Sun, J. Kim, *NPG Asia Mater.* **2014**, *6*, e138.

[66] a) J. Y. Hwang, S. T. Myung, Y. K. Sun, *Adv. Funct. Mater.* **2018**, *28*, 1802938; b) A. Eftekhari, Z. Jian, X. Ji, *ACS Appl. Mater. Interfaces* **2017**, *9*, 4404; c) C. B. Bucur, T. Gregory, A. G. Oliver, J. Muldoon, *J. Phys. Chem. Lett.* **2015**, *6*, 3578.

[67] F. Ye, D. Lu, X. Gui, T. Wang, X. Zhuang, W. Luo, Y. Huang, *J. Materiomics* **2019**, *5*, 344.

[68] P. Vishnuprakash, C. Nithya, M. Premalatha, *Electrochim. Acta* **2019**, *309*, 234.

[69] X. Zhao, X. Zhang, D. Wu, H. Zhang, F. Ding, Z. Zhou, *J. Mater. Chem. A* **2016**, *4*, 16606.

[70] D. Koch, V. V. Kulish, S. Manzhos, *MRS Commun.* **2017**, *7*, 819.

[71] A. Bhatia, J.-P. Pereira-Ramos, N. Emery, R. Baddour-Hadjean, *Chem. Mater.* **2021**, *33*, 5276.

[72] Y. Zhang, X. Niu, L. Tan, L. Deng, S. Jin, L. Zeng, H. Xu, Y. Zhu, *ACS Appl. Mater. Interfaces* **2020**, *12*, 9332.

[73] a) L. Deng, X. Niu, G. Ma, Z. Yang, L. Zeng, Y. Zhu, L. Guo, *Adv. Funct. Mater.* **2018**, *28*, 1800670.; b) Y. Fan, Z. Qu, W. Zhong, Z. Hu, H. A. Younus, C. Yang, X. Wang, S. Zhang, *ACS Appl. Mater.*

Interfaces **2021**, *13*, 7377; c) X. Niu, J. Qu, Y. Hong, L. Deng, R. Wang, M. Feng, J. Wang, L. Zeng, Q. Zhang, L. Guo, Y. Zhu, *J. Mater. Chem. A* **2021**, *9*, 13125.
[74] Y.-H. Zhu, Q. Zhang, X. Yang, E.-Y. Zhao, T. Sun, X.-B. Zhang, S. Wang, X.-Q. Yu, J.-M. Yan, Q. Jiang, *Chem* **2019**, *5*, 168.
[75] K. Yuan, R. Ning, M. Bai, N. Hu, K. Zhang, J. Gu, Q. Li, Y. Huang, C. Shen, K. Xie, *Energy Technol.* **2020**, *8*, 1900796.
[76] C. Liu, S. Luo, H. Huang, Z. Wang, Q. Wang, Y. Zhang, Y. Liu, Y. Zhai, Z. Wang, *J. Power Sources* **2018**, *389*, 77.
[77] B. Tian, W. Tang, C. Su, Y. Li, *ACS Appl. Mater. Interfaces* **2018**, *10*, 642.
[78] X. Liu, G. A. Elia, X. Gao, B. Qin, H. Zhang, S. Passerini, *Batter. Supercaps* **2020**, *3*, 261.
[79] M. Clites, J. L. Hart, M. L. Taheri, E. Pomerantseva, *ACS Energy Lett.* **2018**, *3*, 562.
[80] G. Xu, X. Liu, S. Huang, L. Li, X. Wei, J. Cao, L. Yang, P. K. Chu, *ACS Appl. Mater. Interfaces* **2020**, *12*, 706.
[81] D. S. Charles, F. Guo, X. Shan, S. Kim, Z. W. Lebens-Higgins, W. Xu, D. Su, L. F. J. Piper, X. Teng, *J. Mater. Chem. A* **2021**, *9*, 15629.
[82] D. S. Charles, M. Feygenson, K. Page, J. Neuefeind, W. Xu, X. Teng, *Nat. Commun.* **2017**, *8*, 15520.
[83] Y.-Q. Li, H. Shi, S.-B. Wang, Y.-T. Zhou, Z. Wen, X.-Y. Lang, Q. Jiang, *Nat. Commun.* **2019**, *10*, 4292.
[84] T. D. Gregory, R. J. Hoffman, R. C. Winterton, *J. Electrochem. Soc.* **1990**, *137*, 775.
[85] D. Aurbach, Z. Lu, A. Schechter, Y. Gofer, H. Gizbar, R. Turgeman, Y. Cohen, M. Moshkovich, E. Levi, *Nature* **2000**, *407*, 724.
[86] O. Mizrahi, N. Amir, E. Pollak, O. Chusid, V. Marks, H. Gottlieb, L. Larush, E. Zinigrad, D. Aurbach, *J. Electrochem. Soc.* **2008**, *155*, A103.
[87] H. D. Yoo, I. Shterenberg, Y. Gofer, G. Gershinsky, N. Pour, D. Aurbach, *Energy Environ. Sci.* **2013**, *6*, 2265.
[88] Q. Fu, A. Sarapulova, V. Trouillet, L. Zhu, F. Fauth, S. Mangold, E. Welter, S. Indris, M. Knapp, S. Dsoke, N. Bramnik, H. Ehrenberg, *J. Am. Chem. Soc.* **2019**, *141*, 2305.
[89] a) J. P. Pereira-Ramos, R. Messina, J. Perichon, *J. Electroanal. Chem. Interfacial Electrochem.* **1987**, *218*, 241; b) W.-h Yu, D.-z Wang, B. Zhu, S.-j Wang, L.-x Xue, *Solid State Commun.* **1987**, *61*, 271; c) W.-h Yu, D.-z Wang, B. Zhu, G.-e Zhou, *Solid State Commun.* **1987**, *63*, 1043.
[90] P. G. Bruce, F. Krok, J. Nowinski, V. C. Gibson, K. Tavakkoli, *J. Mater. Chem.* **1991**, *1*, 705.
[91] G. Gershinsky, H. D. Yoo, Y. Gofer, D. Aurbach, *Langmuir* **2013**, *29*, 10964.
[92] A. Mukherjee, S. Taragin, H. Aviv, I. Perelshtein, M. Noked, *Adv. Funct. Mater.* **2020**, *30*, 2003518.
[93] D. Wu, Y. Zhuang, F. Wang, Y. Yang, J. Zeng, J. Zhao, *Nano Res.* **2021**. https://doi.org/10.1007/s12274-021-3679-2
[94] D. Kim, J. H. Ryu, *Electron. Mater. Lett.* **2019**, *15*, 415.
[95] T. S. Arthur, K. Kato, J. Germain, J. Guo, P.-A. Glans, Y.-S. Liu, D. Holmes, X. Fan, F. Mizuno, *Chem. Commun.* **2015**, *51*, 15657.
[96] X. Du, G. Huang, Y. Qin, L. Wang, *RSC Adv.* **2015**, *5*, 76352.
[97] E. Sheha, E. M. Kamar, *Mater. Sci.-Pol.* **2019**, *37*, 570.
[98] V. V. Kulish, S. Manzhos, *RSC Adv.* **2017**, *7*, 18643.
[99] E. A. Esparcia, M. S. Chae, J. D. Ocon, S.-T. Hong, *Chem. Mater.* **2018**, *30*, 3690.
[100] D. Muthuraj, A. Sarkar, M. R. Panda, M. Adil, A. Sagdeo, S. Mitra, *Batter. Supercaps* **2021**, *4*, 1.
[101] L. Yu, X. Zhang, *J. Colloid Interface Sci.* **2004**, *278*, 160.
[102] N. Sa, H. Wang, D. L. Proffit, A. L. Lipson, B. Key, M. Liu, Z. Feng, T. T. Fister, Y. Ren, C. J. Sun, J. T. Vaughey, P. A. Fenter, K. A. Persson, A. K. Burrell, *J. Power Sources* **2016**, *323*, 44.
[103] S. C. Lim, J. Lee, H. H. Kwak, J. W. Heo, M. S. Chae, D. Ahn, Y. H. Jang, H. Lee, S. T. Hong, *Inorg. Chem.* **2017**, *56*, 7668.
[104] R. Verrelli, A. P. Black, C. Pattanathummasid, D. S. Tchitchekova, A. Ponrouch, J. Oró-Solé, C. Frontera, F. Bardé, P. Rozier, M. R. Palacín, *J. Power Sources* **2018**, *407*, 162.
[105] H. D. Yoo, J. R. Jokisaari, Y.-S. Yu, B. J. Kwon, L. Hu, S. Kim, S.-D. Han, M. Lopez, S. H. Lapidus, G. M. Nolis, B. J. Ingram, I. Bolotin, S. Ahmed, R. F. Klie, J. T. Vaughey, T. T. Fister, J. Cabana, *ACS Energy Lett.* **2019**, *4*, 1528.
[106] R. Attias, M. Salama, B. Hirsch, Y. Gofer, D. Aurbach, *ChemElectroChem* **2018**, *5*, 3514.
[107] A. Mukherjee, N. Sa, P. J. Phillips, A. Burrell, J. Vaughey, R. F. Klie, *Chem. Mater.* **2017**, *29*, 2218.
[108] J. L. Andrews, A. Mukherjee, H. D. Yoo, A. Parija, P. M. Marley, S. Fakra, D. Prendergast, J. Cabana, R. F. Klie, S. Banerjee, *Chem* **2018**, *4*, 564.
[109] I. D. Johnson, G. Nolis, L. Yin, H. D. Yoo, P. Parajuli, A. Mukherjee, J. L. Andrews, M. Lopez, R. F. Klie, S. Banerjee, B. J. Ingram, S. Lapidus, J. Cabana, J. A. Darr, *Nanoscale* **2020**, *12*, 22150.
[110] M. Lopez, H. D. Yoo, L. Hu, J. L. Andrews, S. Banerjee, J. Cabana, *ACS Energy Lett.* **2020**, *5*, 3357.
[111] a) M. Inamoto, H. Kurihara, T. Yajima, *Electrochemistry* **2012**, *80*, 421; b) Q. An, Y. Li, H. Deog Yoo, S. Chen, Q. Ru, L. Mai, Y. Yao, *Nano Energy* **2015**, *18*, 265; c) S. Tepavcevic, Y. Liu, D. Zhou, B. Lai, J. Maser, X. Zuo, H. Chan, P. Král, C. S. Johnson, V. Stamenkovic, N. M. Markovic, T. Rajh, *ACS Nano* **2015**, *9*, 8194.
[112] a) L. F. Jiao, H. T. Yuan, Y. J. Wang, H. S. Cao, Y. M. Wang, *Electrochem. Commun.* **2005**, *7*, 431; b) L. F. Jiao, H. T. Yuan, Y. C. Si, Y. J. Wang, J. S. Cao, X. L. Gao, M. Zhao, X. D. Zhou, Y. M. Wang, *J. Power Sources* **2006**, *156*, 673; c) R.-H. Kim, J.-S. Kim, H.-J. Kim, W.-S. Chang, D.-W. Han, S.-S. Lee, S.-G. Doo, *J. Mater. Chem. A* **2014**, *2*, 20636; d) C. L. Zuo, Y. Xiao, X. J. Pan, F. Y. Xiong, W. W. Zhang, J. C. Long, S. J. Dong, Q. Y. An, P. Luo, *ChemSusChem* **2021**, *14*, 2093.
[113] D. B. Le, S. Passerini, F. Coustier, J. Guo, T. Soderstrom, B. B. Owens, W. H. Smyrl, *Chem. Mater.* **1998**, *10*, 682.
[114] D. Imamura, M. Miyayama, M. Hibino, T. Kudo, *J. Electrochem. Soc.* **2003**, *150*, A753.
[115] D. Imamura, *Solid State Ion.* **2003**, *161*, 173.
[116] G. Sai Gautam, P. Canepa, W. D. Richards, R. Malik, G. Ceder, *Nano Lett.* **2016**, *16*, 2426.
[117] N. Sa, T. L. Kinnibrugh, H. Wang, G. Sai Gautam, K. W. Chapman, J. T. Vaughey, B. Key, T. T. Fister, J. W. Freeland, D. L. Proffit, P. J. Chupas, G. Ceder, J. G. Bareno, I. D. Bloom, A. K. Burrell, *Chem. Mater.* **2016**, *28*, 2962.
[118] a) S. H. Lee, R. A. DiLeo, A. C. Marschilok, K. J. Takeuchi, E. S. Takeuchi, *ECS Electrochem. Lett.* **2014**, *3*, 87; b) X. Deng, Y. Xu, Q. An, F. Xiong, S. Tan, L. Wu, L. Mai, *J. Mater. Chem. A* **2019**, *7*, 10644; c) Y. Xu, X. Deng, Q. Li, G. Zhang, F. Xiong, S. Tan, Q. Wei, J. Lu, J. Li, Q. An, L. Mai, *Chem* **2019**, *5*, 1194.
[119] Q. Fu, X. Wu, X. Luo, S. Indris, A. Sarapulova, M. Bauer, Z. Wang, M. Knapp, H. Ehrenberg, Y. Wei, S. Dsoke, *Adv. Funct. Mater.* **2022**, *32*, 2110674.
[120] X. Wang, X. Zhang, G. Zhao, H. Hong, Z. Tang, X. Xu, H. Li, C. Zhi, C. Han, *ACS Nano* **2022**, *16*, 6093.
[121] S. Hou, X. Ji, K. Gaskell, P. Wang, L. Wang, J. Xu, R. Sun, O. Borodin, C. Wang, *Science* **2021**, *374*, 172.
[122] A. Ponrouch, C. Frontera, F. Bardé, M. R. Palacín, *Nat. Mater.* **2016**, *15*, 169.
[123] M. Hayashi, H. Arai, H. Ohtsuka, Y. Sakurai, *J. Power Sources* **2003**, *119-121*, 617.
[124] Y. Murata, S. Takada, T. Obata, T. Tojo, R. Inada, Y. Sakurai, *Electrochim. Acta* **2019**, *294*, 210.
[125] Y. Murata, R. Inada, Y. Sakurai, *J. Electrochem. Soc.* **2021**, *168*, 020528.
[126] T. N. Vo, H. Kim, J. Hur, W. Choi, I. T. Kim, *J. Mater. Chem. A* **2018**, *6*, 22645.

[127] M. Bervas, L. Klein, G. Amatucci, *Solid State Ion.* **2005**, *176*, 2735.
[128] X. Xu, M. Duan, Y. Yue, Q. Li, X. Zhang, L. Wu, P. Wu, B. Song, L. Mai, *ACS Energy Lett.* **2019**, *4*, 1328.
[129] M. S. Chae, J. W. Heo, J. Hyoung, S. T. Hong, *ChemNanoMat* **2020**, *6*, 1049.
[130] L. Liu, Y.-C. Wu, P. Rozier, P.-L. Taberna, P. Simon, H. Yuan, P. Han, K. Tao, S. Liu, E. Gazit, R. Yang, C. J. Liu, N. N. Zhu, J. G. Ma, P. Cheng, Y. Jian, B. Wu, X. Le, Y. Liang, Y. Zhang, D. Zhang, L. Zhang, W. Lu, J. Zhang, T. Chen, J. Jiang, T. Xu, J. Lu, L. Sun, Z. Ni, J. Liu, L. Gu, N. Cui, Q. Xu, Y. Qin, R. Yang, Z. Wu, L. Liu, S. Li, S. Ji, P. Chen, S. Cui, Z. Ma, Y. Weng, Q. Huang, Z. Wu, H. Wu, Y. Lin, R. Fu, H. Lin, X. Tian, P. K. Chu, F. Pan, T. He, B. Lu, Y. Chen, Y. Wang, Y. Zhang, J. L. Davenport, A. P. Chen, C. W. Pao, M. Liu, Z. Sun, A. Stram, A. Mordaunt, J. Velasco, Y. Ping, Y. Zhang, S. Chen, H. Xu, L. Liu, F. Teng, N. Lu, *Research.* **2019**, *2019*, 1.
[131] a) Z. Y. Li, O. Fuhr, M. Fichtner, Z. Zhao-Karger, *Energy Environ. Sci.* **2019**, *12*, 3496; b) A. Shyamsunder, L. E. Blanc, A. Assoud, L. F. Nazar, *ACS Energy Lett.* **2019**, *4*, 2271; c) K. V. Nielson, J. Luo, T. L. Liu, *Batter. Supercaps* **2020**, *3*, 1.
[132] D. Kundu, B. D. Adams, V. Duffort, S. H. Vajargah, L. F. Nazar, *Nat. Energy* **2016**, *1*, 16119.
[133] G. Fang, J. Zhou, A. Pan, S. Liang, *ACS Energy Lett.* **2018**, *3*, 2480.
[134] A. Konarov, N. Voronina, J. H. Jo, Z. Bakenov, Y. K. Sun, S. T. Myung, *ACS Energy Lett.* **2018**, *3*, 2620.
[135] P. Senguttuvan, S.-D. Han, S. Kim, A. L. Lipson, S. Tepavcevic, T. T. Fister, I. D. Bloom, A. K. Burrell, C. S. Johnson, *Adv. Energy Mater.* **2016**, *6*, 1600826.
[136] J. Ding, H. Gao, D. Ji, K. Zhao, S. Wang, F. Cheng, *J. Mater. Chem. A* **2021**, *9*, 5258.
[137] a) J. Ming, J. Guo, C. Xia, W. Wang, H. N. Alshareef, *Mater. Sci. Eng. R Rep.* **2019**, *135*, 58; b) M. Song, H. Tan, D. Chao, H. J. Fan, *Adv. Funct. Mater.* **2018**, *28*, 1802564; c) D. Selvakumaran, A. Pan, S. Liang, G. Cao, *J. Mater. Chem. A* **2019**, *7*, 18209; d) P. Yu, Y. X. Zeng, H. Z. Zhang, M. H. Yu, Y. X. Tong, X. Lu, *Small* **2019**, *15*, 1804760; e) V. Mathew, B. Sambandam, S. Kim, S. Kim, S. Park, S. Lee, M. H. Alfaruqi, V. Soundharrajan, S. Islam, D. Y. Putro, J.-Y. Hwang, Y.-K. Sun, J. Kim, *ACS Energy Lett.* **2020**, *5*, 2376; f) W. Zhang, C. Zuo, C. Tang, W. Tang, B. Lan, X. Fu, S. Dong, P. Luo, *Energy Technol.* **2021**, *9*, 2000789; g) J. Huang, H. Liang, Y. Tang, B. Lu, J. Zhou, S. Liang, *Adv. Energy Mater.* **2022**, *12*, 2201434; h) X. Ma, X. Cao, M. Yao, L. Shan, X. Shi, G. Fang, A. Pan, B. Lu, J. Zhou, S. Liang, *Adv. Mater.* **2022**, *34*, 2105452; i) P. Ruan, S. Liang, B. Lu, H. J. Fan, J. Zhou, *Angew. Chem. Int. Ed.* **2022**, *61*, e202200598.
[138] J. Zhou, L. Shan, Z. Wu, X. Guo, G. Fang, S. Liang, *Chem. Commun.* **2018**, *54*, 4457.
[139] N. Zhang, Y. Dong, M. Jia, X. Bian, Y. Wang, M. Qiu, J. Xu, Y. Liu, L. Jiao, F. Cheng, *ACS Energy Lett.* **2018**, *3*, 1366.
[140] X. Chen, L. Wang, H. Li, F. Cheng, J. Chen, *J. Energy Chem.* **2019**, *38*, 20.
[141] Y. Dong, M. Jia, Y. Wang, J. Xu, Y. Liu, L. Jiao, N. Zhang, *ACS Appl. Energy Mater.* **2020**, *3*, 11183.
[142] R. Li, H. Zhang, Q. Zheng, X. Li, *J. Mater. Chem. A* **2020**, *8*, 5186.
[143] Q. Fu, J. Wang, A. Sarapulova, L. Zhu, A. Missyul, E. Welter, X. Luo, Z. Ding, M. Knapp, H. Ehrenberg, S. Dsoke, *J. Mater. Chem. A* **2021**, *9*, 16776.
[144] P. Byeon, Y. Hong, H. Bin Bae, J. Shin, J. W. Choi, S. Y. Chung, *Nat. Commun.* **2021**, *12*, 4599.
[145] P. Hu, M. Yan, T. Zhu, X. Wang, X. Wei, J. Li, L. Zhou, Z. Li, L. Chen, L. Mai, *ACS Appl. Mater. Interfaces* **2017**, *9*, 42717.
[146] K. Zhu, T. Wu, K. Huang, *Chem. Mater.* **2021**, *33*, 4089.
[147] a) Y. Lu, T. Zhu, W. van den Bergh, M. Stefik, K. Huang, *Angew. Chem. Int. Ed.* **2020**, *59*, 17004; b) X. Chuan, G. Jing, L. Yongjiu, L. Hanfeng, Z. Chao, A. H. N., *Adv. Mater.* **2018**, *30*, 1705580.
[148] a) Y. Yang, Y. Tang, G. Fang, L. Shan, J. Guo, W. Zhang, C. Wang, L. Wang, J. Zhou, S. Liang, *Energy Environ. Sci.* **2018**, *11*, 3157; b) F. Ming, H. Liang, Y. Lei, S. Kandambeth, M. Eddaoudi, H. N. Alshareef, *ACS Energy Lett.* **2018**, *3*, 2602; c) X. Chuan, G. Jing, L. Peng, Z. Xixiang, A. H. N., *Angew. Chem. Int. Ed.* **2018**, *57*, 3943.; d) P. He, G. Zhang, X. Liao, M. Yan, X. Xu, Q. An, J. Liu, L. Mai, *Adv. Energy Mater.* **2018**, *8*, 1702463; e) B. Tang, G. Fang, J. Zhou, L. Wang, Y. Lei, C. Wang, T. Lin, Y. Tang, S. Liang, *Nano Energy* **2018**, *51*, 579; f) X. Wang, B. Xi, X. Ma, Z. Feng, Y. Jia, J. Feng, Y. Qian, S. Xiong, *Nano Lett.* **2020**, *20*, 2899.
[149] a) C. Liu, Z. Neale, J. Zheng, X. Jia, J. Huang, M. Yan, M. Tian, M. Wang, J. Yang, G. Cao, *Energy Environ. Sci.* **2019**, *12*, 2273; b) L. Ma, N. Li, C. Long, B. Dong, D. Fang, Z. Liu, Y. Zhao, X. Li, J. Fan, S. Chen, S. Zhang, C. Zhi, *Adv. Funct. Mater.* **2019**, *29*, 1906142; c) L. Shan, Y. Yang, W. Zhang, H. Chen, G. Fang, J. Zhou, S. Liang, *Energy Storage Mater.* **2019**, *18*, 10; d) J. W. Li, K. McColl, X. K. Lu, S. Sathasivam, H. B. Dong, L. Q. Kang, Z. N. Li, S. Y. Zhao, A. G. Kafizas, R. Wang, D. J. L. Brett, P. R. Shearing, F. Cora, G. J. He, C. J. Carmalt, I. P. Parkin, *Adv. Energy Mater.* **2020**, 10; e) Y. Luo, L. Wei, H. Geng, Y. Zhang, Y. Yang, C. C. Li, *ACS Appl. Mater. Interfaces* **2020**, *12*, 11753.
[150] a) B. Y. Tang, J. Zhou, G. Z. Fang, F. Liu, C. Y. Zhu, C. Wang, A. Q. Pan, S. Q. Liang, *J. Mater. Chem. A* **2019**, *7*, 940; b) X. Wang, B. Xi, Z. Feng, W. Chen, H. Li, Y. Jia, J. Feng, Y. Qian, S. Xiong, *J. Mater. Chem. A* **2019**, *7*, 19130; c) H. Zhao, Q. Fu, D. Yang, A. Sarapulova, Q. Pang, Y. Meng, L. Wei, H. Ehrenberg, Y. Wei, C. Wang, G. Chen, *ACS Nano* **2020**, *9*, 11809.
[151] a) M. S. Javed, H. Lei, Z. Wang, B.-t Liu, X. Cai, W. Mai, *Nano Energy* **2020**, *70*, 104573; b) Y. Li, Z. Huang, P. K. Kalambate, Y. Zhong, Z. Huang, M. Xie, Y. Shen, Y. Huang, *Nano Energy* **2019**, *60*, 752.
[152] a) X. Wang, Y. Li, S. Wang, F. Zhou, P. Das, C. Sun, S. Zheng, Z.-S. Wu, *Adv. Energy Mater.* **2020**, *10*, 2000081; b) D. M. Xu, H. W. Wang, F. Y. Li, Z. C. Guan, R. Wang, B. B. He, Y. S. Gong, X. L. Hu, *Adv. Mater. Interfaces* **2019**, *6*; c) M. Narayanasamy, B. Kirubasankar, M. Shi, S. Velayutham, B. Wang, S. Angaiah, C. Yan, *Chem. Commun.* **2020**, *56*, 6412; d) Y. Tian, Y. An, H. Wei, C. Wei, Y. Tao, Y. Li, B. Xi, S. Xiong, J. Feng, Y. Qian, *Chem. Mater.* **2020**, *32*, 4054.
[153] N. Jayaprakash, S. K. Das, L. A. Archer, *Chem. Commun.* **2011**, *47*, 12610.
[154] M.-C. Lin, M. Gong, B. Lu, Y. Wu, D.-Y. Wang, M. Guan, M. Angell, C. Chen, J. Yang, B.-J. Hwang, H. Dai, *Nature* **2015**, *520*, 324.
[155] L. D. Reed, E. Menke, *J. Electrochem. Soc.* **2013**, *160*, A915.
[156] a) H. Wang, Y. Bai, S. Chen, X. Luo, C. Wu, F. Wu, J. Lu, K. Amine, *ACS Appl. Mater. Interfaces* **2015**, *7*, 80; b) S. Gu, H. Wang, C. Wu, Y. Bai, H. Li, F. Wu, *Energy Storage Mater.* **2017**, *6*, 9; c) A. M. Diem, J. Bill, Z. Burghard, *ACS Appl. Energy Mater.* **2020**, *3*, 4033; d) M. Chiku, H. Takeda, S. Matsumura, E. Higuchi, H. Inoue, *ACS Appl. Mater. Interfaces* **2015**, *7*, 24385; e) N. Canever, T. Nann, *Nano Express* **2020**, *1*, 010016.
[157] T. Das, S. Tosoni, G. Pacchioni, *Comput. Mater. Sci.* **2021**, *191*, 110324.
[158] J. R. González, F. Nacimiento, M. Cabello, R. Alcántara, P. Lavela, J. L. Tirado, *RSC Adv.* **2016**, *6*, 62157.
[159] P. Ruetschi, *J. Power Sources* **1977**, *2*, 3.
[160] Y. Liang, C.-Z. Zhao, H. Yuan, Y. Chen, W. Zhang, J.-Q. Huang, D. Yu, Y. Liu, M.-M. Titirici, Y.-L. Chueh, H. Yu, Q. Zhang, *InfoMat* **2019**, *1*, 6.
[161] R. Benedek, M. M. Thackeray, A. van de Walle, *Chem. Mater.* **2008**, *20*, 5485.
[162] a) Q. Shu, L. Chen, Y. Xia, X. Gong, X. Gu, *J. Phys. Chem. C* **2013**, *117*, 6929; b) H. Pan, Y. Shao, P. Yan, Y. Cheng, K. S. Han, Z. Nie, C. Wang, J. Yang, X. Li, P. Bhattacharya, K. T. Mueller, J. Liu, *Nat.*

Energy **2016**, *1*, 16039; c) W. Sun, F. Wang, S. Hou, C. Yang, X. Fan, Z. Ma, T. Gao, F. Han, R. Hu, M. Zhu, C. Wang, *J. Am. Chem. Soc.* **2017**, *139*, 9775.

[163] a) X. Y. Wu, J. J. Hong, W. Shin, L. Ma, T. C. Liu, X. X. Bi, Y. F. Yuan, Y. T. Qi, T. W. Surta, W. X. Huang, J. Neuefeind, T. P. Wu, P. A. Greaney, J. Lu, X. L. Ji, *Nat. Energy* **2019**, *4*, 123; b) X. Y. Wu, S. Qiu, Y. K. Xu, L. Ma, X. X. Bi, Y. F. Yuan, T. P. Wu, R. Shahbazian-Yassar, J. Lu, X. L. Ji, *ACS Appl. Mater. Interfaces* **2020**, *12*, 9201; c) Y. K. Xu, X. Y. Wu, H. Jiang, L. T. Tang, K. Y. Koga, C. Fang, J. Lu, X. L. Ji, *J. Phys. Chem. C* **2020**, *59*, 22007.

[164] a) J. Choi, E. Alvarez, T. A. Arunkumar, A. Manthiram, *Electrochem. Solid-State Lett.* **2006**, *9*, A241; b) Q. Zhao, L. Liu, J. Yin, J. Zheng, D. Zhang, J. Chen, L. A. Archer, *Angew. Chem. Int. Ed.* **2020**, *59*, 3048.

[165] C. D. Wessells, S. V. Peddada, M. T. McDowell, R. A. Huggins, Y. Cui, *J. Electrochem. Soc.* **2011**, *159*, A98.

[166] a) W. Xu, L. Zhang, K. Zhao, X. Sun, Q. Wu, *Electrochim. Acta* **2020**, *360*, 137008; b) P. Wang, Y. Zhang, Z. Feng, Y. Liu, C. Meng, *J. Colloid Interface Sci.* **2022**, *606*, 1322.

[167] S. Dong, W. Shin, H. Jiang, X. Wu, Z. Li, J. Holoubek, W. F. Stickle, B. Key, C. Liu, J. Lu, P. A. Greaney, X. Zhang, X. Ji, *Chem* **2019**, *5*, 1537.

[168] H. Li, J. Yang, J. Cheng, T. He, B. Wang, *Nano Energy* **2020**, *68*, 104369.

[169] C. Han, J. Zhu, K. Fu, D. Deng, W. Luo, L. Mai, *Chem. Commun.* **2022**, *58*, 791.

[170] Y. Wang, G. Cao, *Chem. Mater.* **2006**, *18*, 2787.

[171] S. Wu, S. Liu, L. Hu, S. Chen, *J. Alloys Compd.* **2021**, *878*, 160324.

[172] a) A. S. Aricò, P. Bruce, B. Scrosati, J.-M. Tarascon, W. van Schalkwijk, *Nat. Mater.* **2005**, *4*, 366; b) C. Jiang, E. Hosono, H. Zhou, *Nano Today* **2006**, *1*, 28.

[173] Y. Ren, A. R. Armstrong, F. Jiao, P. G. Bruce, *J. Am. Chem. Soc.* **2010**, *132*, 996.

[174] a) R. Liu, J. Duay, S. B. Lee, *Chem. Commun.* **2011**, *47*, 1384; b) Z. Chen, Y. Qin, K. Amine, Y. K. Sun, *J. Mater. Chem.* **2010**, *20*, 7606.

[175] a) X. Huang, X. Rui, H. H. Hng, Q. Yan, *Part. Part. Syst. Charact.* **2015**, *32*, 276; b) F. Liu, Z. Chen, G. Fang, Z. Wang, Y. Cai, B. Tang, J. Zhou, S. Liang, *Nano-Micro Lett.* **2019**, *11*, 25; c) X. Liang, L. Yan, W. Li, Y. Bai, C. Zhu, Y. Qiang, B. Xiong, B. Xiang, X. Zou, *Nano Energy* **2021**, *87*, 106164.

[176] H. Zhao, Q. Fu, X. Luo, X. Wu, S. Indris, M. Bauer, Y. Wang, H. Ehrenberg, M. Knapp, Y. Wei, *Energy Storage Mater.* **2022**, *50*, 464.

How to cite this article: Q. Fu, H. Zhao, A. Sarapulova, S. Dsoke, *Appl. Res.* **2022**, e202200070.
https://doi.org/10.1002/appl.202200070